framatome
Framatome GmbH

Abschlussbericht

Final Report

Reaktorsicherheitsforschung - Vorhaben-Nr.: 1501592A

Reactor Safety Research-Project No.: 1501592A

Bruchmechanische Untersuchung von Reaktordruckbehälterstählen mittels Kleinprobentechnik

Fracture mechanics investigation of reactor pressure vessel steels by means of sub-sized specimens

Autoren / Authors:

Florian Obermeier
Hieronymus Hein
Marco Kaiser
Kowalli Philipp
Kuemmel Frank
Rempel Alexey
Bieniek Florian

Dienststelle des Autors / Performing Organisation: Framatome GmbH

Berichtsdatum / Publication Date: 31.05.2023

Das diesem Bericht zugrunde liegende Vorhaben wurde mit Mitteln des Bundesministeriums für Umwelt, Naturschutz, nukleare Sicherheit und Verbraucherschutz (BMUV) unter dem Förderkennzeichen 1501592A gefördert.

Bundesministerium
für Umwelt, Naturschutz, nukleare Sicherheit
und Verbraucherschutz

Hinweis:

Die Verantwortung für den Inhalt dieser Veröffentlichung liegt bei den Autoren.

Framatome GmbH und die Berichtersteller übernehmen keine Haftung für Schäden, die aufgrund von weiterführenden fehlerhaften Anwendungen der in diesem Bericht dargestellten Ergebnisse entstehen.

Kurzfassung

Die strukturelle Integrität des Reaktordruckbehälters (RDB) in Kernkraftwerken muss über die gesamte Lebensdauer und für alle dabei möglichen Lastfälle nachgewiesen werden. Darunter fallen neben dem normalen und gestörten Betrieb auch schwerwiegende Lastfälle wie ein Notkühlszenario mit Thermoschock des RDB. Die Verfahren für die entsprechende sicherheitstechnische Bewertung dieser Ereignisse in Bezug auf den Sprödbruchausschluss des RDBs sind in den länderspezifischen Normen und Regelwerken wie zum Beispiel dem ASME Boiler and Pressure Vessel Code oder den „Sicherheitstechnischen Regeln des kerntechnischen Ausschusses“ KTA vorgegeben und ausführlich beschrieben.

Die grundsätzliche Vorgehensweise ist in den unterschiedlichen Regelwerken vergleichbar. Basierend auf der Berechnung der Spannungsintensität an der Spitze eines konservativ postulierten oder existierenden Fehlers in der RDB Wand, der einem definierten Belastungsszenario ausgesetzt ist, und der experimentell ermittelten Bruchzähigkeit des Materials (Materialwiderstandskurve) wird die Sicherheitsmarge bestimmt. Die Materialwiderstandskurve kann entweder indirekt mittels RT_{NDT} (Reference nil-ductility transition temperature) oder direkt mit dem RT_{T0} Konzept basierend auf dem Master-Curve Ansatz beschrieben werden. Die gebräuchlichsten Probenformen zur Bestimmung der Bruchzähigkeit der Materialien im Ursprungszustand sind dabei die C(T) (Compact Tension) sowie die SE(B) (Single Edge Bend) Probenformen mit 10 mm bis 50 mm Probendicke.

Durch Alterungseffekte, hauptsächlich durch die Bestrahlungsreaktion hervorgerufen, verschlechtert sich die Bruchzähigkeit des Materials. Die Bruchzähigkeitskurve wird dabei während der Betriebsjahre in Richtung höherer Temperaturen verschoben, wodurch sich der Sicherheitsabstand zwischen dieser und der Belastungskurve eines postulierten Fehlers verringert. Um die Verschiebung der Bruchzähigkeitskurve zu messen sind entsprechende Proben Teil der RDB Bestrahlungs-Überwachungsprogramme. Die Überwachungsprogramme wurden so konzipiert, dass sie die Lebensdauer des Kernkraftwerks mit meist 40 Jahren in Bezug auf die erwartete Neutronenversprödung konservativ abdecken. Das dabei verfügbare bestrahlte Material ist im Regelfall begrenzt.

Um einen weiterhin sicheren Betrieb europäischer Kernreaktoren über ursprünglich geplante Laufzeiten hinaus zu gewährleisten, müssen spezifische Probleme gelöst werden, die sich aus der bestrahlungsinduzierten Versprödung von Reaktordruckbehältern (RDB) im Langzeitbetrieb ergeben. Dies erfordert eine Erweiterung der RDB-Bestrahlungsüberwachungsprogramme hin zu längeren Betriebszeiten als ursprünglich geplant. Die bereits angesprochene begrenzte Verfügbarkeit von bestrahltem Material stellt dabei eine große Herausforderung dar.

Die Verwendung der Kleinproben-Versuchstechnik ist eine vielversprechende Option, um diesen Mangel an bestrahltem Material zu umgehen. Durch den Einsatz von Mini-C(T) Proben können aus zwei geprüften Charpy Proben (10 x 10 x 55 mm) bis zu 16 0,16T C(T) Proben mit einer Probendicke von 4 mm hergestellt werden, was eine zuverlässige Bestimmung der Referenztemperatur T_0 nach ASTM E1921 erlaubt. Charpy Proben sind aktuell in den RDB-Bestrahlungsüberwachungsprogrammen weit verbreitet und meist im bereits geprüften Zustand noch verfügbar. So kann dieses Probenmaterial erneut in Bestrahlungsüberwachungskapseln zum Einsatz kommen um auch Fluenzen für den Langzeitbetrieb mit ausreichender Konservativität abzudecken. Die notwendige Bestrahlungsdauer im Vergleich zum Einsatz von gänzlich unbestrahltem Material kann so signifikant reduziert werden. Ein weiterer Vorteil liegt im geringeren Probenvolumen der Mini-C(T) Proben was im bestrahlten Zustand eine geringere Strahlenexposition des Prüfpersonals zur Folge hat.

Über den bereits beschriebenen Einsatz hinaus ergeben sich noch weitere Anwendungsfälle der Kleinprobentechnik wie zum Beispiel eine detailliertere Aussage über den Einfluss der Proben-Entnahmeposition auf die ermittelte Bruchzähigkeit besonders in Bezug auf Schweißgüter.

Um die Akzeptanz für bruchmechanische Prüfungen im spröd-duktilen Übergangsbereich von bestrahlten und nicht bestrahlten RDB-Stählen an Mini-C(T) Proben zu verbessern, wurde ein vom Bundesministerium für Umwelt, Naturschutz, nukleare Sicherheit und Verbraucherschutz (BMUV) mitfinanziertes FuE-Projekt gestartet. Die Partner in diesem Projekt waren die Technische Universität Dresden / Helmholtz-Zentrum Dresden-Rossendorf (HZDR) als Forschungsinstitut sowie die Framatome GmbH als Vertreter der Industrie (kommerzielles Unternehmen in der Kerntechnik / Lieferant).

Dieser Bericht beinhaltet die Arbeiten und Ergebnisse der Framatome GmbH mit der Teilprojekt Nummer 1501592A. Die Arbeiten und Ergebnisse der TU Dresden bzw. des HZDR sind im Bericht zum Teilprojekt 1501592B dokumentiert.

Im Rahmen dieses Teilprojekts wurden zwei unterschiedliche Materialien im Hinblick auf ihre Bruchzähigkeit im Übergangsbereich mittels Mini-C(T) Proben geprüft - jeweils ein Grundwerkstoff und ein Schweißgut im unbestrahlten sowie bestrahlten Zustand. Die Herstellung und Prüfung der Proben erfolgte im Heiße Zellen Labor bzw. dem Werkstoffprüflabor der Framatome GmbH.

Die vier Versuchsreihen bestanden aus jeweils 8 Proben (10 Proben beim unbestrahlten Schweißgut). Im Gegensatz zu den Testreihen basierend auf Bruchmechanikproben mit Standardgrößen, war es in keiner der hier dokumentierten Testreihen möglich auf Basis der 8 Proben eine gültige Referenztemperatur T_0 zu bestimmen. Dies wurde durch eine im Vergleich mit Standardproben relativ hohe Anzahl von Proben verursacht, die die Kriterien der ASTM E1921 im Hinblick auf die Gültigkeit der Rissinitiierungs-Zähigkeit K_{Jc} verletzen. Der Industrieansatz sich bei der Bestimmung der Referenztemperatur T_0 auf 8-10 Proben zu beschränken, was bei normal großen Proben ausreichend ist, ist bei der Verwendung der Mini-C(T) Proben nicht mehr anwendbar. Die Größe eines Prüfloses muss dabei auf mindestens 16 Proben erhöht werden. Der Vergleich der bestimmten T_{0Q} Werte mit den T_0 Werten des Ausgangsmaterials zeigt Differenzen, die sich einerseits mit der zu geringen Anzahl der geprüften Mini-C(T) Proben sowie andererseits durch den Unterschied der Probenform zumindest teilweise erklären lassen.

Eine gute Übereinstimmung wurde bei den Ergebnissen des Grundwerkstoffs im Vergleich mit den Ergebnissen des HZDR erzielt.

Zur Charakterisierung der allgemeinen Eigenschaften der Bruchflächen sowie zur Bestimmung der Lage sowie der Spezifika der Rissinitiierungspunkte wurden fraktographische Untersuchungen durchgeführt. Die Rissinitiierungspunkte wurden mittels Detailaufnahmen (SE/BSE) sowie EDS untersucht. Die Verteilung der Initiierungspunkte der untersuchten Werkstoffe mit einer Häufung im Bereich der Probenmittellinie deckt sich mit den Ergebnissen bereits veröffentlichter Untersuchungen. Ein Einfluss der Seitkerben konnte dabei aufgrund der Probenzahl jedoch nicht bestätigt werden auch wenn die numerischen Untersuchungen dies zeigten.

Um die Übertragbarkeit der Ergebnisse der Mini-C(T) auf Standardproben zu bestätigen, wurden numerische „local approach“ Analysen durchgeführt. Die Ergebnisse zeigen einen leichten aber zu vernachlässigbaren Trend hin zu höheren T_0 Werten bei der Verwendung von größeren Proben. Ebenso konnte die constraint-bedingte T_0 Differenz zwischen SE(B) und C(T) Proben bestätigt werden.

Ein abschließendes Urteil zur Vergleichbarkeit der Ergebnisse der verwendeten Mini-C(T) Proben mit den Ergebnissen von Proben mit Standardgröße konnte wegen der begrenzten Datenbasis in diesem Teilprojekt nicht gefällt werden. Im Rahmen des Teilprojekts mit der FKZ 1501592B wurde jedoch eine deutlich größere Anzahl von Mini-C(T) Proben getestet und eine Vergleichbarkeit der Ergebnisse bestätigt.

Abstract

In order to ensure the continued safe operation of European nuclear reactors, it is necessary to solve specific issues that arise from irradiation induced reactor pressure vessel (RPV) embrittlement under long term operation. This requires an extension of the RPV surveillance programs to cover longer operation times than originally planned. The limited availability of surveillance materials poses a challenge for the feasibility of such programs. Among others, the use of the small specimen technology is a promising option to overcome the lack of materials. For example, 16 sub-sized 0.16T-C(T) specimens (4 mm thickness) can be manufactured from two tested Charpy sized (10 x 10 x 55 mm) specimens, allowing a reliable determination of the reference temperature T_0. Such Charpy sized fracture mechanics specimens are currently widely used in the RPV surveillance programs.

To support the acceptability for fracture mechanics testing of irradiated and unirradiated RPV steels using mini-C(T) specimens, a joined R&D project was launched partly financed by the German Federal Ministry for the Environment, Nature Conservation, Nuclear Safety and Consumer Protection. The partners are the technical University of Dresden / Helmholtz-Zentrum Dresden-Rossendorf (research institutes) and the Framatome GmbH (commercial nuclear company / supplier).

This report covers the work performed at Framatome GmbH, sub-project 1501592A.

Within the scope of this sub-project two different materials have been tested using mini-C(T) specimens - a base material and a weld material both in the unirradiated and irradiated condition. Each test series consisted of 8 (10 for the unirradiated weld material) specimens. In contrast to the use of standard fracture toughness specimens it was not possible to establish a valid T_0 reference with specimen sets of 8 samples in any of the four test series. This was caused by a relatively large number of specimens violating the crack initiation toughness K_{Jc} validity criteria of the testing standard ASTM E1921.

Fractographic examinations on the fracture surfaces of the tested specimens were performed to characterize the general fracture surface characteristics as well as the location and characteristics at the (brittle) crack initiation sites. For this purpose, the crack initiation was characterized with detailed images (SE/BSE) as well as EDS.

To confirm the transferability of results from mini-C(T) specimens to standard specimens a numerical local approach analysis was performed. The results showed a minor trend of a slightly increasing T_0 towards larger specimens and a specimen bias, the difference between SE(B) and C(T) specimens.

A final conclusion on the comparability of mini-C(T) fracture toughness results with results from standard sized specimens cannot be given due to the limited database created within this sub-project. However, in the scope of sub-project FKZ 1501592B a larger amount of mini-C(T) specimens was tested and the comparability was confirmed for the tested materials.

Table of Contents

Abbreviations and Definitions

Abbreviations

ASME	American Society of Mechanical Engineers
ASTM	American Society for Testing and Materials
BM	Base Material
BMUV	Federal Ministry
BSE	Backscattered Electrons
C(T)	Compact Tension
CCA	Compact Crack Arrest
CMOD	Crack Mouth Opening Displacement [mm]
DIN	Deutsches Institut für Normung e.V.
EDM	Electrical Discharge Machining
EDS	Energy-Dispersive X-ray Spectroscopy
EFPD	Effective Full Power Days
EFPY	Effective Full Power Years (=365.25 Days)
ENTENTE	European Database for Multiscale Modelling of Radiation Damage
FAW	Fachanweisung (specific technical instruction)
FEM	Finite Element Method
FKZ	Project number
FRACTESUS	Fracture mechanics testing of irradiated RPV steels by means of sub-sized specimens
HAZ	Heat Affected Zone
JSW	Japan Steel Works
KTA	Kerntechnischer Ausschuss (Nuclear Safety Standards Commission)
KWO	Kernkraftwerk Obrigheim
LA	Local Approach
MeV	Mega electron Volt
LWR	Light Water Reactor
NPP	nuclear power plant
PCCV	Pre-cracked Charpy V-Notch
PTS	Pressurized Thermal Shock
PWR	Pressurized Water Reactor
RDB	Reaktordruckbehälter (Reactor Pressure Vessel)
RPV	Reactor Pressure Vessel
RWE	Rheinisch-Westfälisches Elektrizitätswerk AG
RT	Reference Temperature

SE	Secondary electrons
SE(B)	Single edge bend
SEM	Scanning electron microscopy
VAK	Versuchsatomkraftwerk Kahl (test nuclear power reactor Kahl)
WM	Weld Material
WOL	Wedge Opening Load

Symbol	**Meaning**	**Unit**
a_0	initial crack length	mm
Δa	stable crack growth	mm
E	Young's modulus	MPa
J	J integral	kJ/m^2
K_{Ic}	Static fracture toughness	MPa√m
K_{Jc}	Cleavage crack initiation toughness on the lower shelf and in transition	MPa√m
$K_{Jc(1T)}$	Cleavage crack initiation toughness on the lower shelf and in transition; normalised on standard specimen thickness (1T=25.4mm)	MPa√m
$K_{Jc(Limit)}$	Lower limiting fracture toughness	MPa√m
$R_{p0.2}$	Yield strength	MPa
R_m	Tensile strength	MPa
RT_{T0}	Static fracture toughness Reference Temperature according to the Master curve concept $RT_{T0} = T_0 + 19.4$ K	°C
RT_{NDT}	Reference Nil-Ductility Transition Temperature	°C
RT_{T0}	Static fracture toughness Reference Temperature according to the Master curve concept $RT_{T0} = T_0 + 19.4$ K [°C]	°C
T	Temperature	°C
t	Time	Sec
T_0	Reference Temperature, related to the temperature on the Master curve at which K_{Jc} = 100 MPa√m	°C
T_{0Q}	Invalid Reference Temperature, related to the temperature on the Master curve at which K_{Jc} = 100 MPa√m – too few samples used for the determination	°C
W	Specimen width	mm

Orientation at forgings

T transverse to the main direction of deformation or parallel to the rotational symmetry axis (axial)

L longitudinal to the main direction of deformation

S in thickness direction, perpendicular or radial to the rotational symmetry axis

at welds

L longitudinal to the welding direction

T transverse to the welding direction or parallel to the rotational symmetry axis (axial)

S in thickness direction, perpendicular to the weld

Safety analysis

The safety analysis provides the evidence to exclude the initiation of a brittle failure. Thereby the material characteristic (fracture toughness) is faced to the load characteristic (for postulated disturbances and implied failures). The safety analysis offers the lifetime of the RPV taking the irradiation impact to the material properties into account.

1. Introduction

The structural integrity against brittle fracture of reactor pressure vessels (RPV) operated in nuclear power plants must be proven for the entire lifetime of the component and for all possibly occurring load cases. This includes normal and upset operation conditions as well as severe conditions like a pressurized thermal shock (PTS) event. The procedures for this assessment are provided in several country specific standards like the ASME Boiler and Pressure Vessel Code [1] or the "*Sicherheitstechnische Regeln des kerntechnischen Ausschusses*" KTA [2]. The basics and principles of these procedures are essentially comparable.

In that regard, the margin between the stress intensity at the tip of a conservatively postulated or existing flaw in the RPV wall subjected to a load scenario and the fracture toughness of the material (material resistance curve) has to be determined. This material resistance curve can either be described indirectly, using the RT_{NDT} (reference nil-ductility transition temperature) or directly using the RT_{T0} and fracture mechanics concept based on the Master Curve approach [3], respectively. To measure the fracture toughness of the materials in as received state the most common specimen configurations used are C(T) (compact tension) and SE(B) (single edge bending) with common specimen thicknesses ranging between 10 mm and 50 mm.

Caused by aging effects, mainly irradiation reaction, the fracture toughness of the material will be altered and its fracture toughness curve will be displaced during the service years towards higher temperatures thus reducing the safety. To measure this displacement of the fracture toughness curve as a function of the applied neutron fluence, fracture mechanics specimens are part of the RPV surveillance programs or are manufactured from specimens that are included (e.g. Charpy V-Notch). In general, the available irradiated material is very limited and sometimes just sufficient to determine a valid reference temperature. Thus, the RPV surveillance programs were designed to cover the entire lifetime and expected fluences of a nuclear RPV with a common design life of 40 years of operation.

However, some nuclear power plants aim to increase their lifetime, in some cases up to 80 years. In order to ensure continued safe operation in regards of this so called long-term operation (LTO) it is necessary to solve specific issues that arise from irradiation induced RPV embrittlement. It requires an extension of the RPV surveillance programs to cover this extension of the lifetime beyond the original design life.

To address this issue of generally limited irradiated material and to provide an option to reinsert already irradiated and tested specimens in surveillance capsules for further irradiation and retesting at higher fluence levels corresponding to long term operation conditions the small-scale specimen technology is a promising option.

In this work miniature compact tension (mini-C(T)) specimens with a 4 mm specimen thickness (0.16T) were used to perform fracture toughness testing according to ASTM E1921 [4]. The small size of the specimens allows to reuse already tested material from single edge bend SE(B) or Charpy sized specimens with the common dimensions of 10 x 10 x 55 mm for the manufacturing of eight 0.16T C(T) specimens.

2. Project planning and implementation

2.1. Scientific and technical work objectives

The purpose of this research project is to develop and validate a methodology to determine fracture mechanical properties of unirradiated and irradiated RPV materials based on mini-C(T) specimens, see Figure 1.

The following objectives shall be addressed:

- Establishing a new or confirming existing procedures for the fracture mechanics testing of unirradiated and irradiated RPV steels using small scale specimens (mini-C(T)) technique including manufacturing, fatigue pre-cracking and measuring of the crack opening displacement.
- Investigation of the fracture mechanic properties as a function of the neutron fluence.
- Assessment of the transferability of fracture mechanic results from small scale specimens to specimens with different size and scale.

The project is carried out as a joint research project with the project partners TU Dresden / Helmholtz Zentrum Dresden Rossendorf (HZDR) covering sub-project 1501592B and Framatome GmbH covering sub-project 1501592A. This report covers the work performed by Framatome GmbH.

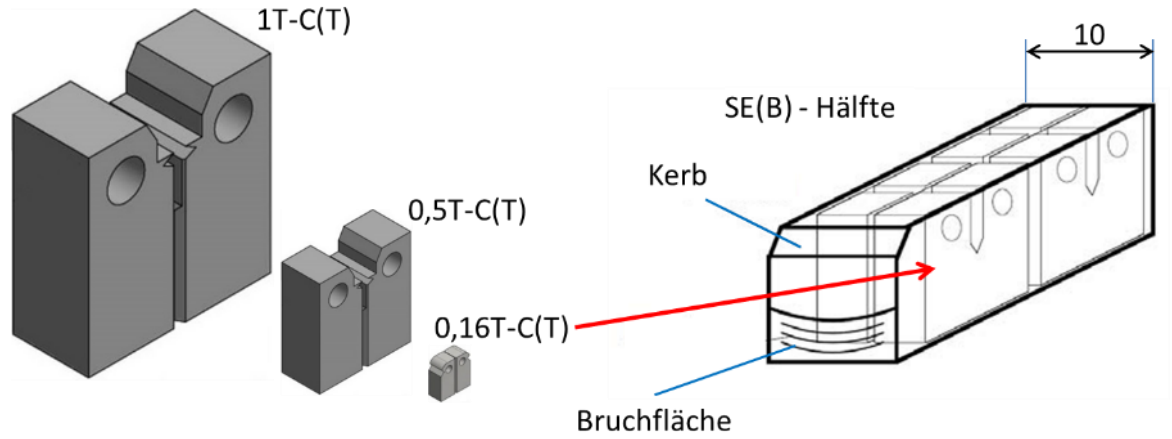

Figure 1: Size comparison between standard sized fracture mechanics specimens and 0.16T C(T) miniature specimens

2.2. Work plan

To address the described objectives, the joint R&D project was organized in seven work packages (WP). The work packages WP1, WP2, WP3 and WP4 were jointly processed by TU Dresden and Framatome GmbH likewise. The distribution of sample manufacturing, testing and evaluation to two laboratories was mainly driven by capacity and time constraints. In addition, this allowed a comparison between the accredited test laboratories at Framatome GmbH and a laboratory with a scientific orientation at TU-Dresden/HZDR, which provided additional security for the results obtained. WP5 was processed by Framatome GmbH only.

- WP0: Project Management and Coordination

The project management was divided into a superordinate project management, carried out by Framatome GmbH and a subordinate technical project management for planning, coordination and dispatching of the work in the two institutions. The preparation and execution of the project meetings was also part of this non-technical WP.

- WP1: Manufacturing of the sub sized 0.16T C(T) samples

The 0.16T C(T) samples were manufactured from tested standard samples of RDB steels that were both irradiated and unirradiated. For irradiated materials, the manufacturing process took place in the hot cells. The original planned sample matrix for Framatome GmbH is shown below.

Table 1: Planned Framatome GmbH sample matrix

Material	Origin	Fluence	Number and Orientation of samples
22 NiMoCr3-7	Framatome Stock,	unirradiated	8 x T-L
Base Material	Irradiated in VAK	285 °C / 4.0E19 cm^{-2} (E > 1 MeV)	8 x T-L
S3NiMo1	Framatome Stock,	unirradiated	8 x T-L
Weld Material	Irradiated in VAK	285 °C / 5.0E19 cm^{-2} (E > 1 MeV)	8 x T-L

The weld material in this matrix was later changed to NiCrMo1 due to limitations in the availability of the S3NiMo1 material. The material matrix of the TU-Dresden/HZDR is not shown here.

- WP2: Determination of the T_0 reference temperature according to the Master Curve concept

The testing of the irradiated specimens was performed in the hot cells environment of Framatome GmbH and the HZDR. The unirradiated specimens were tested in the conventional labs. Testing and evaluation of the reference temperature has been performed according to ASTM E1921.

- WP3: Fractography of the samples

After fracture toughness testing of the specimens, scanning electron microscopy (SEM) was used to examine the fracture surface for cleavage fracture and to determine the crack initiation positions.

- WP4: Comparison between standard-sized and mini-C(T)

Within this WP the fracture toughness and reference temperature results of the mini-C(T) specimens were compared to the already existing results from larger specimens.

- WP5: Numerical simulations and local approach

This WP was intended to support the design of the experiments and their evaluation using finite element methods (FEM). Local approach calculations should demonstrate the transferability of the results generated by testing sub-sized specimens to standard specimens and thus prove the application in safety assessments

- WP6: Documentation

2.2.1. Materials

The experimental test matrix of the sub-project consisted of two RPV materials being representative for European light water reactors (LWR). A base material (BM) with optimized chemical composition as well as a weld material (WM) with higher susceptibility for irradiation embrittlement was chosen which is caused by higher contents of copper.

- P7 BM / ANP-3
  22 NiMoCr3-7 (forged ring, quenched and tempered, corresponds to ASTM A 508 Grade 2, manufactured by Klöckner)
  - Part of prior fracture toughness related R&D programs (CARISMA [5], CARINA [6] & CAMERA [7])
  - Existing Master Curve data for the unirradiated condition as well as several fluences ($4.45 \cdot 10^{19}$, $3.73 \cdot 10^{19}$, $4.26 \cdot 10^{19}$ n/cm^2 (E > 1 MeV))
- P370 WM / ANP-5
  NiCrMo1 UP/LW320, LW330 (higher copper content, modified manufacture, annealed) for generic examinations
  - Part of prior fracture toughness related R&D programs (CARISMA [5], CARINA [6] & CAMERA [7])
  - Existing Master Curve data for the unirradiated condition as well two fluences ($2.21 \cdot 10^{19}$, $2.25 \cdot 10^{19}$ n/cm^2 (E > 1 MeV))

During the application phase of the project, it was planned to perform testing on the following weld material showing a high susceptibility for irradiation embrittlement due to a high nickel content.

- P16 WM / ANP-6
  - Part of prior fracture toughness related R&D programs (CARISMA [5], CARINA [6] & CAMERA [7])
  - Existing Master Curve data for the unirradiated condition as well as several fluences ($7.43 \cdot 10^{18}$, $8.36 \cdot 10^{18}$, $4.60 \cdot 10^{19}$, $5.43 \cdot 10^{19}$ n/cm^2 (E > 1 MeV))

Due to limitations in the availability of this material in the unirradiated condition the P370 WM was chosen instead. Both weld materials show a comparable high susceptibility for irradiation embrittlement - the P370 WM due to the high copper content and the P16 WM due to the high nickel content.

The P16 WM specimens GS72 and GS73 with fluencies of $4.79 \cdot 10^{19}$ and $4.86 \cdot 10^{19}$ n/cm^2 were sent to HZDR to complement the material already available there. The results are covered in the final report of sub-project 1501592B [8].

Table 2 shows the chemical composition of the used materials. The composition of the P16 WM is shown for comparison as well albeit not tested in the Framatome scope of the project.

Table 2: Chemical composition [7]

Material	Specifiaction	Manufacturing Type	C [%]	Si [%]	Mn [%]	P [%]	S [%]	Cr [%]	Mo [%]	Ni [%]	Cu [%]	V [%]	Ta [%]	Co [%]	Al [%]
P7 BM	22NiMoCr3-7 Kloeckner	forged ring	0.240	0.200	0.720	0.015	0.014	0.430	0.790	0.970	0.120	-	0.010	0.015	0.027
P370 WM	NiCrMo1 UP (mod) LW320, LW330	submerged arc welding	0.080	0.150	1.140	0.015	0.013	0.740	0.600	1.110	0.220	0.010	-	-	0.013
P16 WM	S3NiMo3/OP41TT Uddcomb	submerged arc welding	0.050	0.150	1.410	0.012	0.007	0.070	0.460	1.690	0.080	0.004	0.002	0.024	0.022

Table 3 and Table 4 shows the T_0 transition temperature results available prior to this project

Table 3: T_0 transition temperature [5]

Material	Fluence E>1MeV [cm^{-2}]	Orientation	T_0 [°C]	Valid/Invalid	Used Specimen	Reference
P7 BM	0.00E+00	T-L	-88	valid	SE(B) 10x10	[5]
	4.45E+19	T-L	-22	valid	PCCV	
P370 WM	0.00E+00	T-L	-38	valid	SE(B) 10x10	[5]
	2.12E+19	T-L	103	invalid	WOL 100X	
	2.25E+19	T-L	102	valid	PCCV	
P16 WM	6.21E+18	T-L	-10	invalid	WOL 25X	[5]
	8.36E+18	T-L	-36	valid	PCCV	

Table 4: Tensile Properties [5], [6]

Material	Fluence E>1MeV [cm^{-2}]	Temp [°C]	$R_{eH}/R_{P0.2}$ [MPa]	R_m [MPa]	Reference
P7 BM	0	-196	963	1011	[5]
		-150	726	856	
		-100	593	762	
		-50	501	687	
		22	450	610	
		275	404	573	
	3.81E+19	-100	730	845	[5]
		-50	670	782	
		25	598	718	
P370	0	-140	822	892	[5]
		-100	724	812	
		-50	822	740	
		20	604	696	
		150	546	623	
		280	534	616	
	2.16E+19	25	821	860	[5]
		50	783	832	
		75	772	823	
		275	669	757	
P16 WM	0	-196		992	[5]
		-150	775	833	
		-100	665	760	
		-50	606	700	
		22	555	632	
		100	527	583	
		200	476	550	
		300	483	563	
	7.27E+18	23	628	713	[6]
		150	530	622	
		275	535	633	
	4.65E+19	-100	977	982	[5]
		-50	879	911	
		25	817	842	

2.2.2. Representativeness

The tested materials are identical or “production compliant” with original RPV materials from German pressurized water reactors (PWR) and can be assigned to the following generations:

- P7 BM: 22NiMoCr3-7 (manufactured by Klöckner)
  1st and 2nd generation (Obrigheim, Stade, Biblis A, Biblis B, Unterweser, Neckarwestheim 1)
- P370 WM: NiCrMo1 UP (modified) /LW320, LW330
  1st generation (Obrigheim, Stade)
- P16 WM: S3NiMo/OP41 TT UP-WM (Uddcomb-Fertigung)
  3rd generation (Vorkonvoi, Grafenrheinfeld, Brokdorf)

2.2.3. Source material & origin

To demonstrate the material reusability advantage of the small scale 0.16T C(T) specimens SE(B), Charpy V-Notch and Compact Crack Arrest (CCA) specimens have been used as source material that have already been tested in precursor R&D projects.

The source for the P7 BM in the unirradiated condition is two SE(B) specimens designated SEB1 and SEB2 that have been tested in the framework of the CAMERA R&D project [7] in accordance with ASTM E1921 following a warm-prestress loading. The irradiated P7 material was provided in the form of two tested Charpy V-Notch specimens [5] designated BA25 with a fluence of 3.86E+19·cm^{-2} (E > 1 MeV) and BA26 with a fluence of 3.95E+19·cm^{-2} (E > 1Mev). The Charpy specimen BA21 with a fluence of 3.95E+19·cm^{-2} (E > 1 MeV) has been sent to HZDR for investigation.

The source for the P370 WM in the unirradiated condition is a compact crack arrest specimen (CCA) designated CD8M3 tested in the framework of the CARINA R&D project [6]. The irradiated P370 weld material was provided in the form of two tested Charpy V-Notch specimens designated D37 with a fluence of 2.30E+19·cm^{-2} (E > 1 MeV) and D85 with a fluence of 2.24E+19·cm^{-2} (E > 1Mev). D37 has been tested during project CARISMA [5] as a Charpy test and D85 during project CAMERA [7] as a fracture toughness specimen in the ductile region following ASTM E1820 [4].

The source for the P16 weld material in the irradiated condition, sent to HZDR, is two SE(B) specimens tested following ASTM E1921 in the framework of project CARINA [6]. The two specimens are designated GS72 with a fluence of 4.79E+19·cm^{-2} (E > 1 MeV) and GS 73 with a fluence of 4.86E+19·cm^{-2} (E > 1 MeV) and have been manufactured from one untested WOL 100X specimen GS7. Testing provided the fracture toughness values K_{Jc} of 107 MPa√m (GS72) tested at 120 °C and 92.1 MPa√m (GS73) tested at 110 °C.

2.2.4. Irradiation of samples and applied neutron fluence

The materials investigated in this project were pre-irradiated in the test nuclear power plant Kahl (VAK) at temperatures between 280 °C ≤ T ≤ 290 °C in the frame of several dedicated irradiation surveillance programs in the 1980s.

The VAK reactor, a small experimental boiling water reactor operated by RWE with an electrical output of approx. 15 MW, has been operated until 1985. Between 1975 and 1985 it was also used by Siemens/KWU as an irradiation plant for various research and irradiation surveillance programs. The neutron spectrum of the VAK reactor was comparable to that of other PWRs of Siemens/KWU; the neutron flux density at the capsule positions was approx. $2 \cdot 10^{12}$ cm^{-2}s^{-1} (E > 1 MeV). For the various types of irradiation studies an irradiation temperature

between 265 °C and 316 °C was used. Originally, the VAK RPV was equipped with 12 capsule supports for irradiation purposes, which were later supplemented by three further inner irradiation positions at 90°, 180° and 270°, so as to enable irradiation of large capsules of 965 mm in length and 100 mm x 146.5 mm in cross-section (meeting the dimensions of the WOL 100X specimens). Between 1981 and 1985, the VAK reactor was used to irradiate RPV material samples from the German PWR construction lines for storage purposes, so as to enable examination of their long-term irradiation behaviour and to safeguard the integrity of the RPVs with regard to later changes and possible long-term operation [6].

In the years 1983 and 1985, a total of 6 large-capacity VAK capsules with all in all 39 WOL 100X, 60 Pellini, 48 tensile and 765 Charpy specimens were irradiated. In the course of these irradiation activities, the source material samples for P7 BM and P16 WM were irradiated in the large capacity capsules KA6 and KA4 under the following irradiation conditions [6]:

- Capsule KA4 irradiated at position 90° from 1983-09-08 until 1983-10-23 (44.6 EFPD)
- Capsule KA6 irradiated at position 270° from 1985-01-19 until 1985-09-29 (246.5 EFPD)

The sample material P370 WM was irradiated in the VAK capsule KWO 01 at position 90° from 1980-11-26 until 1981-03-29 (122 EFPD).

After irradiation, the VAK capsules with the samples were transported to the “Hot Cell” test laboratory of KWU in Erlangen where they were stored in a shielded storage rack.

Details about the disassembly of the irradiation capsules and the determination of the neutron fluences may be found in reference [7].

3. State of the art

According to national standards a brittle fracture safety analysis is to be performed for any operating nuclear RPV. The deterministic concepts developed in the 1970s to assess safety against brittle failure of the RPV are mainly based on experience, that brittle failure of the material can be described as a function of temperature by and experimentally verified limit curve of the fracture toughness K_{Ic}, with A, B and C being material-dependent parameters.

$$KIc = A + B \cdot \exp(C \cdot T) \quad (1)$$

This limit curve determined on unirradiated materials is shifted to higher temperatures on the temperature axis for the irradiated material state due to neutron irradiation induced embrittlement of the material. The amount of the shift has been determined through Charpy impact testing on materials in the as-received state and in the irradiated state as well [2] & [3].

Besides the described deterministic approach, a fracture mechanics-based reference temperature concept was established for the safety assessment that is based on the statistical Master Curve concept [3] & [9]. Based on this concept the test standard ASTM E1921 has been developed. It describes a method for the direct determination of the reference temperature T_0 from fracture mechanics testing.

The Master Curve concept was developed and validated using fracture mechanical tests on standardized samples (e.g., 1T C(T), 0.5T C(T), SE(B) 10x10 mm). The planned reuse of already tested standard samples as part of the extension of the surveillance programmes raises the question of the transferability of the Master Curve method to miniature samples.

In principle, the fracture toughness values from different samples sizes can be normalized to the standard size of 25.4 mm (1T) [3]:

$$K_{Jc}^{(X)} = K_{min} + (K_{Jc}^{(0)} - K_{\min}) \cdot \left(\frac{B_0}{B_x}\right)^{1/4} \quad (2)$$

$$K_{min} = 20MPa\sqrt{m}\,, \qquad B_0 = 25.4\,mm$$

B_x is defined by the specimen thickness. However, this conversion for very small samples (B < 10 mm) is not sufficiently proved with experimental fracture mechanics data.

Furthermore, the applicability of miniature fracture toughness samples must be proven because of the validity criterion for the specimen limit load given in the ASTM E1921:

$$K_{Jc(limit)} = \sqrt{\frac{E \cdot b_0 \cdot \sigma_y}{M}} \quad (3)$$

Formula (3) describes the calculation of the $K_{Jc(limit)}$ using the Young's Modulus E, the ligament b_0, the yield strength σ_y and the constant M (=30). According ASTM E1921 the ligament is proportional to the specimen thickness. The measuring capacity $K_{Jc(limit)}$ of a sample therefore decreases with decreasing sample size. As a consequence, small samples may need to be tested at lower temperatures compared to normal sized specimen, to obtain a valid K_{Jc} datum. However, this may violate another condition of the Master Curve methodology, namely that a valid transition temperature T_0 can only be determined if sufficient underlying KJc values are available in the temperature interval.

$$T_0 - 50K \leq T \leq T_0 + 50K \quad (4)$$

Another aspect is the possibly lower constraint (strain restriction in thickness direction) of small samples. The Master Curve methodology assumes a plane strain condition in the sample, so that the crack initiation sites along the fatigue crack front should in principle be evenly distributed. However, finite element analyses have shown, that the crack driving force along the crack front increases towards the center of the specimen and the distribution of the initiation site should reflect that.

Furthermore, due to the plastic deformation at the crack tip with increasing K_I it is more likely to reduce the constraint in small samples compared to larger samples [10] & [11].

If the plane strain condition is not sufficient a higher concentration of the crack initiation points in the specimen center can be expected, which may be accompanied by an overestimation of the K_{Jc} values.

Hence, the transferability of the fracture toughness obtained from small sized samples like 0.16T C(T) to standard sized samples needs to be demonstrated.

There are already some fracture toughness results from small scale specimens available using mostly unirradiated materials. At the initiative of the Japanese CRIEPI institute, an inter-laboratory comparison using 0.16T C(T) samples was carried out in 2014, in which the HZDR was involved [12]. The principal applicability of the Master Curve method was demonstrated. However, a slight dependence of the determined reference temperature T_0 on the selected test temperature was observed. It has also been shown, that due to the reduced fracture toughness measuring capacity of the small samples compared to standard samples, the test temperatures must be chosen at least 20 K lower than the expected reference temperature T_0.

The applicability was also proven for weldments [13]. In particular, it was shown that the Weibull exponent of m = 4 is valid for this geometry. Investigations on the statistical distribution of the position of the crack initiation points along the crack front showed a concentration of the initiation points in the middle of the sample at higher load levels. Different geometries of the used side grooves showed no significant effect [14].

Further investigations on the comparability of the small sample results with standard samples, carried out on a Japanese RPV base material SFVQ1A (ASME A508 Cl.3) in the irradiated state, also demonstrated the fundamental suitability of the small samples. However, the results showed a 14 °C lower reference temperature compared to 0.5T C(T) samples. The authors of the study referred to statistical effects with regard to this difference and recommended an increase of the minimum quantity of valid samples necessary for a valid evaluation of the fracture toughness [15].

For a further inter-laboratory comparison, a European base material comparable to ASTM A533 Grade B Class 1 was used in the unirradiated and irradiated state [16]. The reference temperature was determined according to ASTM E1921 using 0.16T C(T) samples and compared with results measured on PCCV (Pre-Cracked Charpy V-Notch) samples. In the unirradiated state an approximately identical reference temperature was determined. In the irradiated state, the largest difference between PCCV and 0.16T C(T) results was 12 °C.

In order to prove the applicability to weldments, tests were carried out in 2017 on a weldment with a characteristically low upper-shelf temperature (Linde 80 WF-70) in the unirradiated condition [17]. The used material was part of the Midland RPV core weld characterization program, an unfinished U.S nuclear reactor. The conclusion of this study was, that 0.16T C(T) specimens are also suitable for fracture mechanics tests on weldments, but recommends to significantly increase the number of specimens used for the determination of the reference temperature. In addition to this study, experiments were conducted on specimens in the irradiated condition [18]. Out of 15 tested specimens, 3 provided invalid results and 4 violated the validity criteria of ASTM E1921 for $K_{Jc(limit)}$ or stable crack growth. Again, the author concluded that a significantly higher number of 0.16T C(T) specimens is required compared to the conventional specimen sizes. The results in for the unirradiated state showed a very good comparison of the measured reference temperature

with only 1 °C difference to result from standard samples. However, for the irradiated condition the 0.16T C(T) samples provided a reference temperature of 15 °C or 25 °C lower compared to standard samples, depending on the used censoring method.

The material of the irradiated Midland core weld was tested by two other laboratories with test series of 15 samples each [19]. In both cases, the number of samples that violated the ASTM 1921 validity criteria and had therefore to be considered invalid or censored was comparatively high. As a result, it was not possible to determine a valid reference temperature for a test series based on 15 samples. For the second test series it was possible to determine a valid reference temperature. However, 5 samples violating the criterion for stable crack growth were included in the evaluation as censored values.

A summary evaluation of the fracture mechanics investigations of the midland core weld based on 0.16T C(T) samples yielded a reference temperature T_0 of 13.2 °C or 17.5 °C depending on the censoring method used (including non-cleavage results as censored values or not including them) [20]. This is at least 11.5 °C lower compared with the reference temperature T_0 of 29 °C measured at 1T C(T), 0.5T C(T) and PCCV samples reported in [18]. The results of 50 0.16T C(T) samples were used in this summary evaluation with 14 violating the stable crack growth criterion and 6 the $K_{Jc(limit)}$ criterion.

The applicability of the mini-C(T) specimens in the reference temperature T_0 concept has been advanced internationally in recent years. Although the results so far have been promising, some questions remain unanswered:

- The rather high number of samples that violate the validity criteria of ASTM E1921 which can adversely affect the determined reference temperature.
- The explanation of the differences in the irradiation induced shift in fracture toughness which some test series show, comparing mini-C(T) with standard specimen.
- Limited number of available results on the irradiated material and especially irradiated and unirradiated weld metals.
- The general transferability of the results to standard samples and hence, to component safety assessments.

4. Experimental studies and obtained results

4.1. Provision and manufacturing of specimens

Manufacturing of all irradiated and unirradiated samples was performed in the Hot Cells laboratories of Framatome GmbH. The unirradiated samples were used in this context to prepare for the more complicated manufacturing of the irradiated ones.

The manufacturing of the 34 0.16T C(T) specimens was executed following the design drawing shown in Attachment 1. A 0.2 mm step was planned on the top face of the samples to account for and remove possible irregularities on the corresponding face of the parent specimen, dents from Charpy testing for example.

In the following passages it is described how the sampling took place using the example of the SE(B) 10x10 specimen D73.

In the first step, the specimen side opposite the dovetail of the SE(B) 10x10 specimen was marked with the letters that will be attached to the previous SE(B) specimen identification, in this case A to H like shown in Figure 2.

Figure 2: Re-stamping of sample D73

In the next production step, the starter bore holes were set for the subsequent production of the contour using wire electrical discharge machining (EDM) Figure 3.

Figure 3: Placement of the starter bore holes for EDM

The following Figure 4 shows specimen D73F as an example for all the manufactured 0.16T C(T) specimens.

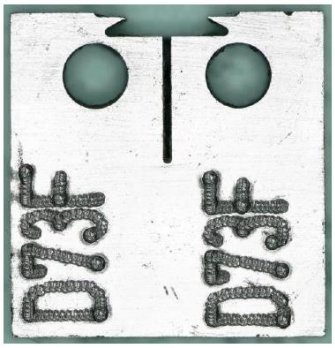

Figure 4: 0.16T C(T) sample D73F

The procedure described above applied for the manufacturing of the P7 BM specimens in unirradiated and irradiated condition and also for the P370 WM specimens in irradiated condition. The P370 WM specimens in the unirradiated condition were manufactured from a broken CCA specimen and will not be described in detail here as the single steps are essentially identical besides the different source sample.

After the manufacturing of the contours a fatigue pre-crack needed to be introduced into the specimens. By high frequency vibration stress on a resonance testing machine, the crack introduced by EDM was extended to an average value of the initial crack length a_0 of 5 mm, so that a ratio between a_0 and the sample thickness W (a_0/W ratio) of 0.5 (0.45 to 0.55 is to be achieved according to ASTM E1921 [4]). In order to be able to visually control and measure the crack elongation during fatigue pre-cracking by either a video system for the irradiated specimens or directly for the unirradiated ones, the area around the fatigue pre-crack needed to be polished beforehand.

Two 45° side-grooves with an 0.5 mm notch radius were inserted in the crack plane of the specimen sides, so that a test ready 0.16T C(T) with an exact net sample thickness B_N of 3.2 mm was produced.

During the course of this project a link was established with the EU R&D project FRACTESUS (Euratom grand agreement No. 900014) to exchange experience and results. One of the early outcomes of this link was the decision to change from side-grooved samples to samples without side-grooves since it was expected, that this has a negligible effect on the results but reduces the complexity of manufacturing irradiated specimen. This decision was made after manufacturing has already started.

In the following table of the manufactured samples a column is included to account for this change, Table 5.

Table 5: Manufactured 0.16T C(T) samples and their origin

Material	Sample Origin Information							Project Data			
	Sampel Type	Orientation	Number	Designation	Capsule	Fluence	T_0	Number	0.16T C(T) sample designation	Orientation	Sidegrooves
P370 SG	CCA	T-L	One Halve	CD8M.3	---	---	-60 °C	10	8M.3A 8M.3B 8M.3C 8M.3D 8M.3E 8M.3F 8M.3G 8M.3H 8M.3J 8M.3L	T-L	no
	SE(B) 10x10	T-L	Both halves	D73	KWO1	2.30E+19	102 °C	8	D73A D73B D73C D73D D73E D73F D73G D73H	T-L	yes yes no no no yes yes yes
P7 GW	SE(B) 10x10	T-L	Both halves	SEB1	---	---	-88 °C	8	SEB1A SEB1B SEB1C SEB1D SEB1E SEB1F SEB1G SEB1H	T-L	no
	Charpy-V	T-L	Both halves	BA25	KA6	3.86E+19	-21,5 °C	8	BA25A BA25B BA25C BA25D BA25E BA25F BA25G BA25H	T-L	yes no no no yes yes yes yes

4.1.1. Design of the specimen

For measuring the LLD of the 0.16T C(T) specimens during testing, three basic options exist. To measure the LLD directly in the load line either by applying the clips on the inside of the sample (see Figure 5, left), or on the outside of the specimen. The third option is to measure the CMOD on the top face of the specimen and convert the measurement afterwards to LLD. Which design to choose depends on the resources available (clip gauge design) at the labs and the overall lab conditions or requirements. Since the clip gauge design available at Framatome GmbH Labs only allowed for a measurement from the inside of the specimen the design to measure LLD from the outside surfaces of the sample were rejected. Due to the simpler application of the clip at the top face of the samples in view of a hot cells environment an application at the LLD on the inner surface was rejected as well. The conversions from CMOD at the top face of the sample to LLD are described in chapters 4.2.1 and 4.2.3.

Figure 5: 0.16T C(T) design discussed at Framatome GmbH

4.2. Fracture toughness testing according to ASTM E 1921

4.2.1. Test procedure

The irradiated and unirradiated samples were tested in the Hot Cells and conventional testing laboratories according to ASTM E1921 [4] standard. The design of the 0.16T C(T) samples, albeit small in comparison to standard sized specimens is specified in the standard. Also specified is specimen preparation, testing conditions and the evaluation procedure of the fracture mechanical characteristic values.

The tests were carried out in the tensile area of class 1 ball-screw testing machines. The acceptance of the testing machines with a force transducer was carried out in accordance to DIN EN ISO 7500-1 [22].

The transducers have been calibrated according to DIN EN ISO 9513 [23] and their suitability for the registration of the sample expansion regarding linearity and resolution at different temperatures has been verified and documented.

The crack mouth opening displacement (CMOD) diagrams were recorded at a displacement-controlled speed of 0.1 mm/min (constant cross-head velocity) for the unirradiated samples and 0.2 mm/min for the irradiated samples. These testing speeds yielded a load rate of approx. 0.2 to 0.7 MPa√m/s (target range according to [4] 0.1 to 2 MPa√m/s).

The crack opening displacements in the load plane (LLD) was calculated based on the CMOD determined during the test. The arrangement of the transducer cutting edges on the top face of the sample was chosen because the arms of the clip would have hit the inner surface of the sample in case of a load line placement, which would have endangered the secure fit of the clip during the test, see also chapter 4.1 for manufacturing details. In addition, this position also provided a higher resolution of the clip due to the larger displacement. For the calculation of LLD based on the measured CMOD a fixed factor of 0.769 was used for the irradiated samples. For the unirradiated samples a correction was used following an internal procedure, Report No. 1:

$$\frac{X_0}{W} = 0.1 + 0.9 \cdot \frac{a_0}{W} \tag{5}$$

$$\frac{CMOD}{LLD} = (X_0 + X)/X_0 \tag{6}$$

with *X* being the distance between load line and CMOD measurement position on the front face.

After examination of the specimens and full opening in liquid nitrogen where necessary, the broken specimen halves were measured with regard to the shape of their pre-crack according to ASTM E1921 [4] on nine defined positions by means of contact-free digital photography and measurement. These measurement results were transferred from the measuring program directly into an evaluation table and provided the subsequent overall evaluation of the crack front. To calculate the fracture toughness limit according to ASTM E1921 [4], the corresponding yield strength values from tensile tests are required as a function of the test temperature. Arbitrary test temperature dependent yield strength values were determined using the Zerilli Armstrong correlation [24]. After verification of the validity criteria, the test analysis and calculation of characteristic values was performed according to ASTM E1921 and with the help of a validated Excel spreadsheet calculation program. This evaluation protocol also documents the specimen dimensions and all relevant measured values of the force-displacement recordings and the measured crack geometry.

4.2.2. Test results

The evaluation and analysis of the $K_{Jc(1T)}$ values and the determination of the Master Curve were performed according to test standard ASTM E1921 version 19b. In the following versions of the ASTM E1921 some changes were made, specifically in the treatment of the crack front straightness validity criterion. These changes and their impact will be addressed after the presentation of the initial test results generated with ASTM E1921-19b, in chapter 4.2.3.

P7 BM unirradiated condition

Four samples out of eight tested samples provided a valid K_{Jc}. The four invalid samples violated the specimen limit criterion. Based on these results a T_{OQ} of -111.6 °C was calculated. Attachment 2 shows the corresponding Master Curve diagram.

P7 BM $3.86 \cdot 10^{19}$ cm^{-2} (E > 1MeV)

Out of 8 tested samples only 3 samples provided a valid K_{Jc}. Three samples violated the criteria for specimen limit with two samples also violating the stable crack growth validity criterion and two samples the criterion for a straight crack-front according to ASTM E1921-19b. Based on these results a T_{OQ} of -41.3 °C was calculated. Attachment 3 shows the corresponding Master Curve diagram.

P370 WM unirradiated condition

Six out of ten tested samples provided a valid K_{Jc} value. Two samples violated the criterion for stable crack growth a_{pmax} and two samples did not break. A T_{OQ} of -7.9 °C was calculated based on these results. Attachment 4 shows the corresponding Master Curve diagram.

P370 WM $2.30 \cdot 10^{19}$ cm^{-2} (E > 1MeV)

Five of the eight tested samples provided a valid K_{JC} value. One sample violated the criterion for a straight crack front and samples D73G and D73E the criterion for stable crack growth. Based on the results a T_{0Q} of 129.6 °C was calculated. Attachment 5 shows the corresponding Master Curve diagram.

4.2.3. Reassessment following ASTM E1921 version 22

To account for changes in the ASTM E1921 version 20 to version 21 a reassessment of the fracture toughness results was performed using the most recent version available at the time this report was created, version 22.

These changes mainly affect the treatment of the validity criterion for a straight crack front. In the earlier versions of the standard the criterion was checked by measuring the fatigue pre-crack length a_0 at "*nine equally spaced points centred about the specimen centreline and extending to 0.01 B from the free surface of plane specimens or near the side groove roots on side grooved specimens".* If one of these nine measurements differed by more than $0.1(b_0B_N)^{1/2}$ from the average value, the evaluated K_{Jc} datum was supposed to be treated as invalid.

From version 21 on a passage was added excluding the two near-surface pre-crack measurement points from this assessment. Based on this change, three more samples from this projects' scope can be treated as valid.

- P370 WM unirradiated condition
  - D73D
- P7 BM irradiated condition
  - BA25B, BA25C

In addition, the calculation of the LLD based on the measured CMOD was updated using the approach given in the ASTM E1921 standard. Following the standard, the LLD can be determined by multiplying the CMOD measured at the front face of the specimen (at 0.25*W* in front of the load line) by a constant factor of 0.73 [3]. This conversion method is based on the virtual rotation point in front of the specimens' crack tip and has the form of equation (7).

$$\frac{LLD}{CMOD} = \frac{a_0 + r \cdot (W - a_0)}{a_0 + r \cdot (W - a_0) + X} \tag{7}$$

With:

X = Distance between load line and CMOD measurement position

r = proportional rotation point (0.365) [25]

However, in the presented case, the measurement of CMOD was not performed on the front face of the specimen, which is 2 mm apart from the load line, but at 1.8 mm distanced from the load line providing a constant correction factor of 0.75.

The effect of the CMOD to LLD conversion on the K_{JC} estimation and hence on the reference temperature T_0 can be expected to be small. However, in some cases where the K_{Jc} value is close to the $K_{Jc(Limit)}$ value of the sample this conversion can be critical if a sample must be censored or not and hence also have an increased effect on the determination of T_0.

In the presented case the P7 BM sample SEB1C is affected, turning from a valid K_{Jc} datum into a datum censored to $K_{Jc(Limit)}$ and therefore having a larger impact on the determination of the reference temperature T_{0Q}.

The following list summarizes the changes in T_{0Q}

- P7 BM unirradiated condition
  - -111.6 °C -> -116.2 °C
- P7 BM irradiated condition
  - -41.3 °C -> -37.3 °C
- P370 WM unirradiated condition
  - -7.9 °C -> -9.3 °C

- P370 WM irradiated condition
  - 129.6 °C -> 129.9 °C

The corresponding master curves to this reassessment are shown in Attachment 6 to Attachment 9.

4.2.4. Assessment using only valid samples

Compared to the usage of standard sized specimen like 1T C(T) or 0.5T C(T) samples the used sample size in this study of 0.16T C(T) specimens produces a larger amount of K_{Jc} datum that need to be censored in relation to valid K_{Jc} datum. This censoring is caused by samples violating the specimen limit load criterion, the stable crack growth criterion or both.

The following table provides an overview based on the reassessment of chapter 4.2.3 showing a range of 25 - 62.5% censored datum for the dataset of this study.

Table 6: Numbers of valid, censored and invalid samples

Material	Fluence			Censored		
	[cm^{-2}] E>1MeV	Total	Valid	Limit load	Stable crack growth	Limit load and stable crack growth
P7 BM	0.00E+00	8	3	5	0	0
	3.86E+19	8	5	1	0	2
P370 WM	0.00E+00	8	6	0	1	1
	2.30E+19	8	6	0	0	2

To highlight the influence of these censored values, a T_0 assessment was performed utilizing the valid samples only providing the following T_{0Q} datum:

- P7 BM unirradiated
  - T_{0Q} = -82 °C (based on 3 valid results)
- P7 BM irradiated
  - T_{0Q} = -20.8 °C (based on 5 valid results)
- P370 WM unirradiated
  - T_{0Q} = -4.8 °C (based on 5 valid results, one result out of ± 50°C temperature range)
- P370 WM unirradiated
  - T_{0Q} = 135 °C (based on 3 valid results, three results out of ± 50°C temperature range)

Focusing on strictly valid results in the determination of the base materials' reference temperature T_{0Q} provides results that are closer to the reference temperature results from standard sized specimen. In case of the weld material the trend is reversed and the results deviate even more from the ones of standard specimen.

However, the number of samples tested in this study proved insufficient to determine a reliable T_0 reference temperature. Therefore, the statement about the effect of larger amounts of censored values within a given dataset should be handled with caution.

4.2.5. Summary and discussion

Table 7 provides a summary of the fracture toughness testing results together with the reference results obtained with larger specimens. In none of the available test series a valid reference temperature T_0 according to ASTM E1921 could be generated with the sample base of 8 (10 in case of the P370 base material).

Table 7: Summarized reference temperature T_0 results

	Reference results			Results of the present study				
Material	Fluence E>1MeV [cm^{-2}]	Orientation	T_0 [°C]	Fluence E>1MeV [cm^{-2}]	Orientation	T_{0Q} 1921-19b [°C]	T_{0Q} 1921-22 [°C]	T_{0Q} Valid samples only [°C]
P7 BM	0.00E+00	T-L	-88	0.00E+00	T-L	-111.6	-116.2	-82
	4.45E+19	T-L	-22	3.86E+19	T-L	-41.3	-37.3	-20.8
P370 WM	0.00E+00	T-L	-38	0.00E+00	T-L	-7.9	-9.3	-4.8
	2.25E+19	T-L	102	2.30E+19	T-L	129.6	129.9	135

P7 BM

The T_{0Q} calculated following ASTM E1921-22 (chapter 4.2.3) values deviate by -28.2 °C in the unirradiated condition and by -15.3 °C in the irradiated condition from the reference results.

P370 WM

The T_{0Q} calculated following ASTM E1921-22 (chapter 4.2.3) values deviate by +28.7 °C in the unirradiated condition and by +27.9 °C in the irradiated condition from the reference results.

For the industrial application of the ASTM E1921 eight samples per test series proved to be the sweet spot between achievable result and effort respectively costs using standard specimen like SE(B) 10x10 or 1T C(T) for example. Already at the beginning of this project it was expected that this number would no longer be sufficient for the use of 0.16T C(T) specimens. The tests carried out now confirmed this assumption. In none of the four test series a valid T_0 could be determined. The calculated T_{0Q} values deviated from the expected values by up to -28.2 °C in the base material and +27.9 °C in the weld metal. The removal of the relatively high number of censored results from the evaluation of base metals T_{0Q} provided results almost identical to the expected ones. However, this does not apply for the weld metal. Here the difference increases even further. This can be explained by the nature of the censored values, which usually reduce the conservatism of the reference temperature in terms of providing lower T_0 values. Based on these observations it can be expected that a larger sample set used during testing of the base material could have provided comparable results. However, this is not to be expected with regard to the weld material.

A summary of the fracture toughness results as well as all relevant input parameters for the determination of the reference temperature T_0 is provided in Attachment 10.

4.2.6. Storage of the test specimens

All material samples tested have been intermediately stored in the material testing laboratory of Framatome GmbH (unirradiated state) and in the safe of the “Hot Cell” test laboratory (irradiated state) until further use.

4.2.7. Inter-laboratory comparison

The P7 BM was also investigated by the project partner HZDR as an inter-laboratory comparison with the results of the HZDR documented in reference [8]. The HZDR tested 16 specimens in both conditions, unirradiated as well as irradiated. In the irradiated condition 11 specimens

provided valid results in addition to 4 censored ones and one invalid due to an irregular crack front after fatigue pre-cracking. In the unirradiated condition 11 specimens provided valid results and 5 needed to be censored. These results were sufficient to calculate valid reference temperatures T_0 with -98.8 °C in the unirradiated condition and -38.8 °C in the irradiated condition.

Combining the results of both labs to one reference temperature evaluation provides the T_0 values of -105.1 °C in the unirradiated condition and -39 °C in the irradiated condition, see Attachment 11 and Attachment 12. The K_{Jc} values in the diagrams show, that the results of both laboratories are essentially comparable. However, the calculated T_0 values of the combined results are in both conditions 17 °C less conservative than the reference values. Part of this difference could be explained by the difference in specimen geometry used between the reference solution (SE(B)) and the specimen type used in this project.

However, removing the censored K_{Jc} values from the reference temperature evaluation provides quite comparable results with the reference solution.

Table 8: Inter-Laboratory Comparison

	Reference results			Results of the present study					
Material	Fluence E>1MeV [cm^{-2}]	Orientation	T_0 [°C]	Fluence E>1MeV [cm^{-2}]	Orientation	Framatome [°C]	HZDR [°C]	Combined [°C]	Combinded only valid [°C]
P7 BM	0.00E+00	T-L	-88	0.00E+00	T-L	-116.2	-98.8	-105.1	-86.6
	4.45E+19	T-L	-22	3.86E+19	T-L	-37.3	-38.8	-39	-25.3

4.3. Fractographic examinations

4.3.1. Test procedure

The following procedures were used, of which not all were within the scope of the accreditation according to DIN EN ISO 17025: 2018 [26] as per annex to the accreditation certificate D-PL-21039-03-00.

- Macrofractographic examination of the fracture surface using a stereomicroscope (not accredited)
- Microfractographic examination of the fracture surface using a SEM (not accredited)
- Microanalysis in the scanning and transmission electron microscope (EDS) in accordance to FAW-M 0012 Rev. D (accredited method)

The aim of the fractographic examinations of the tested 0.16T C(T) samples is to characterize the general fracture surface characteristics as well as the location and characteristics at the (brittle) crack initiation sites. For this purpose, the crack initiation was characterized with detailed images (SE/BSE) as well as EDS. In addition, the distance of the crack initiation to the pre-crack end and the lateral position with respect to the side surface (not the lateral notch ground) were determined. In case of ductile failure, the fracture surface was documented with overview images and detail images.

4.3.2. Test results

4.3.2.1. Fracture surface characteristics

An overview of the fracture surface and the results from the fracture surface characteristic analysis of the different samples is shown in Attachment 13 to Attachment 22.

4.3.2.2. Initiation sites

The results from the crack initiation site characteristic analysis as well as the position of the crack initiation is shown in Attachment 23 to Attachment 26.

4.3.2.3. Summary and discussion

The fracture surfaces of the four different materials were investigated which have been tested following ASTM E1921 at different temperatures:

- Weld material P370:
  - Sample names: 8M.3X
  - Test temperature range: - 60 °C ≤ T ≤ -20 °C
- Base material P7:
  - Sample names: SEB1X
  - Test temperature range: - 125 °C ≤ T ≤ -110 °C
- Weld material P370 irradiated:
  - Sample names: D73X
  - Test temperature range: 80 °C ≤ T ≤ 95 °C
- Weld material P7 irradiated:
  - Sample names: BA25X
  - Test temperature range; - 55 °C ≤ T ≤ -40 °C

Fracture surface characteristics:

- The fracture mode in the base metals (samples SEB1X and BA25X) is mostly cleavage fracture for all samples tested in the given temperature range.
- The main fracture mode in the weld materials changed in the investigated temperature range. However, the fracture surface is quite inhomogeneous in some samples with presence of other fracture modes in some areas.
  - Samples 8M.3X: mostly cleavage fracture was observed at temperatures lower than -45 °C; at temperatures higher than -40 °C it was mostly dimple fracture.
  - Samples D73X: mostly cleavage fracture was observed at temperatures lower than 85 °C; at temperatures higher than 90 °C mostly dimple fracture.

Crack initiation site characteristics

- Samples 8M3X: Crack initiation at MnSiAl-rich Oxide- inclusion in 6 of 10 samples.
- Samples SEB1X: Crack initiation at predominantly grain boundaries. Only in minor cases at inclusions.

- Sample D73X: Crack initiation at MnSiAl-rich Oxide-inclusions in 4 of 8 samples.
- Samples BA25X: Crack initiation at predominantly grain boundaries. Only in minor cases at inclusions.
- Weak trend of an increasing crack initiation distance and mean stretch zone width with increasing testing temperature in weld metals
- The crack initiation site is predominantly located close to the lateral center of the samples Figure 6. No clear trend difference between side grooved and non-side grooved specimen visible.

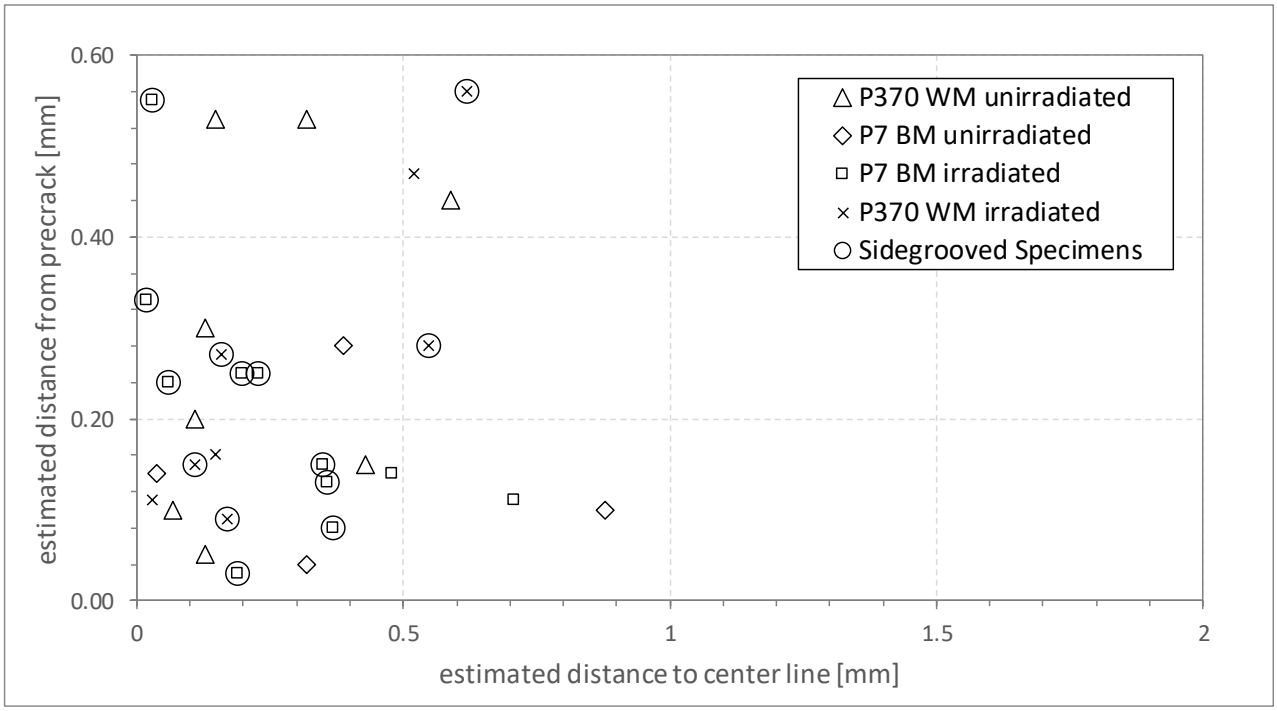

Figure 6: Location of the crack initiaion site of the different analyzed samples

4.3.3. Storage of the test specimens

All material samples tested have been intermediately stored in the material testing laboratory of Framatome GmbH (unirradiated state) and in the safe of the “Hot Cell” test laboratory (irradiated state) until further use.

5. Numerical calculations

5.1. Demonstration of the transferability

The transferability of fracture toughness test results between different sample sizes is crucial for the application in safety assessments. The ASTM E1921 accounts for different sample sizes (size effect) by providing a normalization to 1T (25.4 mm) specimen thickness.

The demonstration that this normalization is applicable to sub-sized sample as well, a local approach (LA) model was used able to describe the local damage mechanism and hence the failure probability in the brittle to ductile transition regime independent from the sample geometry.

5.1.1. Description of the local approach model

Besides the global fracture mechanics concepts like the stress intensity factor K or the J-Integral which are based on macroscopic mechanisms there are the so-called micromechanical models. These models use local mechanisms and are based on the failure mechanisms that are actually occurring within the material. These characteristics enable to describe the failure behaviour independent from the geometry and make these models applicable to small sized specimens and complex component structures likewise.

The local approach model to describe the behaviour of ferritic steels in the brittle and brittle to ductile transition region is based on the work performed by Beremin [28] and [29] with minor modifications implemented within Framatome GmbH. It considers the two relevant damage mechanisms, the creation of micro cracks and their spreading into the material matrix. Based on the local plastic deformation of the matrix material the enclosed brittle particles crack accompanied by a release of stored strain energy. This crack grows into the matrix if the released energy is high enough. At this point the crack either blunts or grows even further. In general brittle failure is based on the so-called weakest link theory. The global integrity is directly related to the integrity of each potential micro crack. The first micro crack that does not blunt will cause global collapse. Both initiation and propagation processes occur statistically based on the local plastic strains and stresses and will lead to failure of the specimen or component with a certain probability. The Local Approach model used here is programmed to provide a global probability of failure of the specimen under investigation that can be directly related to a J-Integral or the stress intensity value.

The calculation of the probability of failure P_f and the corresponding Weibull stress σ_w will be explained briefly within the next few passages.

The global probability of failure based on the so-called Weibull stress is defined as:

$$P_f(\sigma_w) = 1 - \exp\left(-\left(\frac{\sigma_w}{\sigma_u}\right)^m\right) \tag{8}$$

σ_u and m are model parameters. The Weibull stress is determined based on the stress and strain field calculated using numerical simulation. According to Bordet the Weibull stress is assembled by the two terms for crack initiation and propagation.

$$\sigma_w = \left(\int_{V_p} \int_0^{\varepsilon_{p,u}} \frac{{\sigma_{ys}}^2(T,\dot{\varepsilon}_p)}{\sigma_{ys,0}} \exp\left(-\frac{\sigma_{ys}(T,\dot{\varepsilon}_p)}{\sigma_{ys,0}} * \frac{\varepsilon_p}{\varepsilon_{p,0}}\right) \left(\sigma_1^m(\varepsilon_p, dV) - \sigma_{th}^m\right) d\varepsilon_p \frac{dV}{V_0} \right)^{\gamma_m} \tag{9}$$

$\varepsilon_{p,0}$ and σ_{th} are also two model parameters that need to be determined. The calculation of the Weibull stress includes the consideration of the whole load history of a potential micro crack. This is calculated by the integration of the local failure probability over the plastic deformation from zero to a finite value. The calculation of the global Weibull stress is done by integration of the local parameters of all potential micro cracks along the relevant zone of the crack front. This process zone Vp is described by three criteria:

- $\sigma_I > \sigma_{th}$
- $\sigma_{Mises} > \sigma_{Yield}$
- $\Delta\varepsilon_p > 0$

These criteria ensure that for a given place and a given time increment plastic deformation occurs and the prerequisites for crack initiation are given.

To account for the warm pre-stress effect, the Weibull stress formulation of Bordet was modified to account for a temperature change in space and time. To consider the temperature dependent yield strength of the material it is necessary to calculate the probability of crack initiation incrementally.

$$\sigma_w^* = \left(\int_{V_p} \int_0^{\varepsilon_p(t)} \frac{\sigma_{ys}^2(T,\dot{\varepsilon}_p)}{\sigma_{ys,0}} \left(\sigma_1^m(\varepsilon_p, dV) - \sigma_{th}^m\right)\left(1\text{-}P_{nuc}(t)\right) \frac{d\varepsilon_p}{\varepsilon_{p,0}} \frac{dV}{V_0} \right)^{1/m} \quad (10)$$

$$P_{nuc}(t) = 0$$

for t = 0

$$P_{nuc}(t+\delta t) = P_{nuc}(t) + \left(1 - P_{nuc}(t)\right) * \frac{\sigma_{ys}}{\sigma_{ys,0}} * \frac{\varepsilon_p(t+\delta t) - \varepsilon_p(t)}{\varepsilon_{p,0}}$$

for t > 0

A more detailed explanation of this model and the modifications can be found in the deliverables of the PERFORM 60 project [30].

5.1.2. Calibration of the model parameters

The calibration of the basic model parameters was performed within the European R&D project PERFORM 60 [30]. Based on this calibration it is possible to consider most ferritic steels by knowing the difference between the calibration material (P147 BM) and the material under investigation regarding its yield stress at room temperature in the state of interest (unirradiated / irradiated). To check and adjust this calibration isothermal local approach calculations were performed for each of the three investigated materials at different temperatures and the calculated failure probabilities were compared with failure probabilities given by the corresponding Master Curve.

5.1.3. Approach

Two numerical models were prepared for different specimen sizes, one with a sharp crack for the calculation of the J-Integral, and a second one with a blunt crack, used to determine the stresses and strains required for the local approach assessment. The specimen types and sizes calculated were as follows:

- SE(B) 10x10
- 0.16T C(T) (with and without side grooves)
- 0.4T C(T)
- 1T C(T)

For the creation of the geometric as well as finite element models the commercial finite element software ABAQUS CAE version 2017 [31] was used. The models were created as quarter models to take advantage of the symmetrical character of the specimen geometries. A hard-frictionless contact formulation was used between the specimen and the simulated loading bolt. The 3D solid meshes consisted of hexahedral elements using quadratic form functions. The areas around the crack tips were modelled using fully integrated 20-noded brick elements (C3D20) with a highly refined mesh to capture the J-Integral as well as the stress and strain fields accurately. The remaining regions were meshed using 20-noded brick elements with reduced integration (C3D20R). The SE(B)10x10, the 0.4T C(T) and the 1T C(T) specimens were modelled with side

rooves, the 0.16T C(T) specimen without. Figure 7 shows an example of the SE(B) specimen mesh on the left and a C(T) specimen mesh on the right.

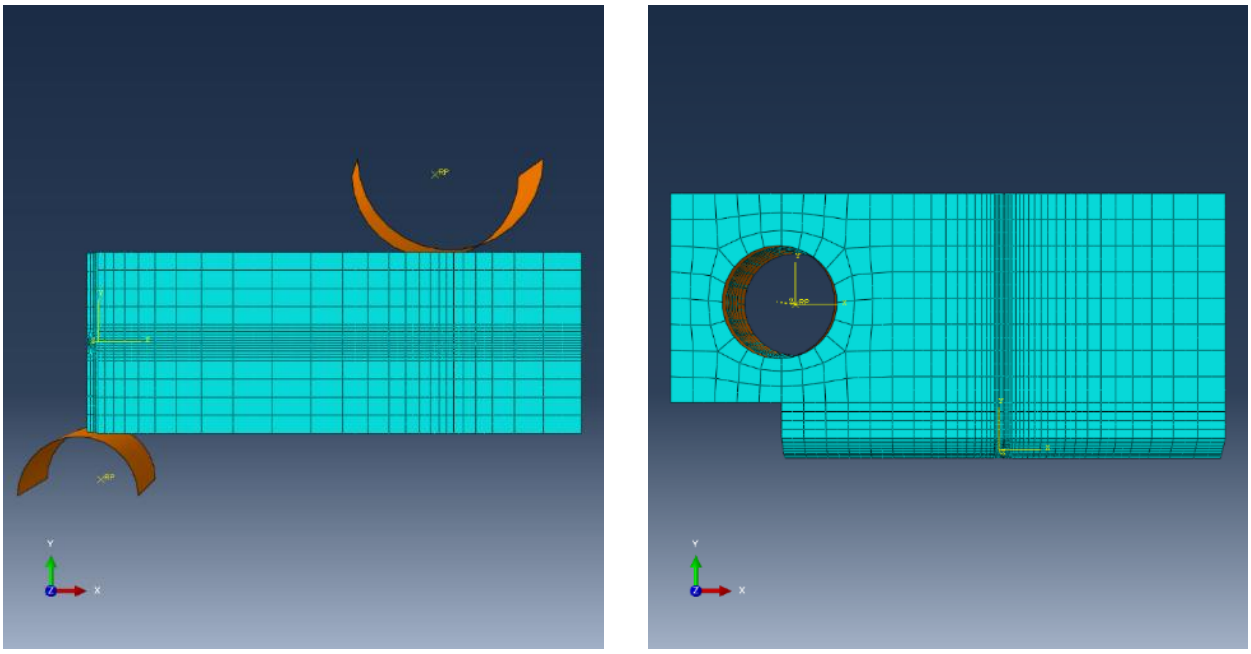

Figure 7: Example of SE(B) left and C(T) specimen mesh right

Figure 8 shows an example of the sharp crack tip for J-Integral evaluation on the left and a blunt crack mesh for stress and strain evaluation to determine the Weibull-stress on the right.

For the demonstration of the transferability the material properties of P370 WM in the irradiated condition were used. The local approach model was calibrated to the transition temperature T_0 of the SE(B) sample set with a fluence of 2.25E+19 cm^{-2} (E > 1 MeV). The following list summarizes the calibrated as well as the fixed LA parameters:

m	= 6.36	$\sigma_{u,const}$	= 1369.3
σ_{th}	= 1546	$\sigma_{u,exp}$	= 633.4
ep_0	= 0.165	C	= 0.0129

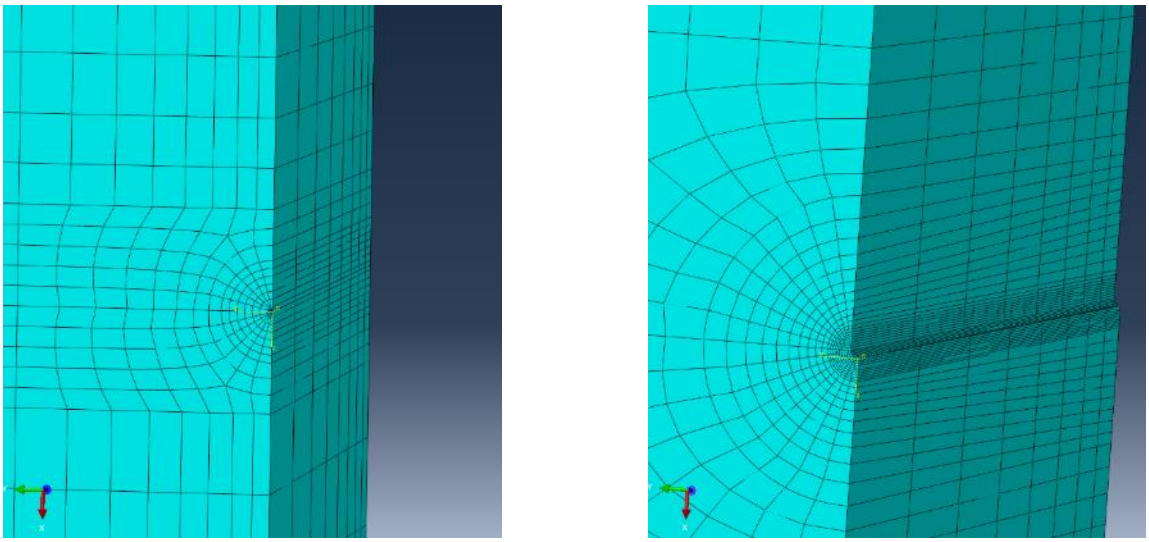

Figure 8: Crack tip mesh; sharp crack for J-Integral evaluation on the left; blunt crack for stresses and strains on the right

5.1.4. Results

The combination of the J-integral calculations with the local approach calculations provides a failure probability as a function of the fracture toughness K_J, derived from J. Based on K_J at 50% failure probability the T_0 – local approach was calculated following formula (11).

$$T_0 = \frac{ln\left(\frac{K_J - 30}{70}\right)}{0.019} - T \tag{11}$$

The SE(B) specimen was analysed in detail as it has already been used during the calibration process. Here the failure probabilities and fracture toughness results are available at 5 temperatures, Attachment 27. For the 0.16T C(T) specimen calculations have been performed at four temperatures each. For the remaining specimen geometries only results at the temperature of 100 °C were calculated, close to the expected reference temperature.

The results of the calculated local approach reference temperatures are as follows:

SE(B) 10x10 (reference solution):	98.2 °C
0.16T C(T) without side grooves:	105.5 °C
0.16T C(T) with side grooves:	105.7 °C
0.4T C(T)	106.2 °C
1T C(T)	106.8 °C

A slight trend is noticeable within the C(T) geometry specimen towards higher values with increasing specimen size. Comparing the SE(B) geometry results with the 0.4T C(T) results (same specimen thickness) shows a difference of 8 °C caused by the different geometry, specifically the higher geometrical constraint of the C(T) specimen. This difference is known as the specimen bias effect and has already been described in reference [3] with a difference of 8 °C ± 15 °C and the ASTM E1921 standard, in which a difference of 10 °C is given. *“On average, T_0 values obtained from C(T) specimens are higher than T_0 values obtained from SE(B) specimens. Best estimate comparison indicates that the average difference between C(T) and SE(B)-derived T_0 values is approximately 10 °C”.*

The results of the local approach analysis show, that despite the comparably small size of the 0.16T C(T) specimens the transferability of results to larger specimens is given. Hence, results from 0.16T C(T) specimens can be used in nuclear RPV brittle fracture safety assessments as well.

6. Conclusion

During fracture toughness testing it became apparent, that the common industrial approach to concentrate on material test series of testing 8 to 10 samples for a valid T_0 does not hold for 0.16T C(T) specimens. It was not possible to determine a valid T_0 in any of the four conducted test series. In comparison with standard specimens a relatively large number of samples violated the validity criteria of the ASTM E1921 and had to be censored or declared invalid. This was already expected at the beginning of the project and documented in references [12] to [20]. A recommendation should be provided in the test standard to increase the number of samples in test series to at least 16 maybe even more for weld materials if tested with 0.16T C(T) specimen size.

The determined T_{0Q} showed a significant difference to the expected T_0 values measured on standard sized specimens. Some of this difference could be the somewhat low statistical foundation of the T_{0Q} values and the influence of a larger amount of censored KJC values on small datasets. Some difference could also be explained with the specimen bias effect (constraint difference between SE(B) and C(T) specimens) accounting for ~ 10 °C of the difference. Guidelines should be implemented in the ASTM E1921 how to treat datasets with an unusual high amount of censored K_{Jc} values. The reason for the difference of the weld material results in irradiated as well as unirradiated conditions with and T_{OQ} increase of approximately +30 °C (non-conservative) in both conditions despite the evaluation approach however, need to be further clarified.

Both laboratories were able to produce comparable results in the case of the P7 BM. A combination of the results provided in both the unirradiated state as well as the irradiated state a difference of -17 °C compared to the reference solution which could be explained by the different specimen geometries used for the reference solution (SE(B)) and this project. However, removing the relatively high number of censored values from the reference temperature calculation provides quite comparable results with the reference solution. Guidance in the test standard ASTM E 1921 is necessary on how to approach data sets with an unusual high amount of censored K_{Jc} values.

The local approach assessment showed, that a transferability of fracture toughness results from mini-C(T) specimens to standard sized specimens is given and hence the possible applicability of such results in brittle fracture safety analyses of nuclear RPVs. The analysis also confirmed the specimen bias effect as documented in [3] and [4].

A weak trend of an increasing crack initiation distance and mean stretch zone width with increasing testing temperature was detected in the weld metal during the fractographic analyses. The crack initiation sites found were predominantly located close to the lateral center of the samples with no clear trend difference between side grooved and non-side grooved specimens visible. The distribution of the initiation sites is in general comparable to distributions documented in reference [14].

During the project period, a link was established to the EU project FRACTESUS. Some of the experimental results gained within this project were exchanged with FRACTESUS.

A final conclusion on the comparability of mini-C(T) fracture toughness results with results from standard sized specimens cannot be given due to the limited database of this sub-project. However, in the scope of sub-project FKZ 1501592B a larger amount of mini-C(T) specimens was tested and the comparability was confirmed for the tested materials.

Acknowledgements

We acknowledge the financial support of this research by the German BMUV, project “Kleinproben” (FKZ 1501592A). The support from the project management organisation (GRS) is also gratefully acknowledged.

7. References

[1] ASME Boiler & Pressure Vessel Code
Section XI, Rules for in-service inspection of nuclear power plant components, 2007

[2] Safety Standards of the KTA
Components of the Reactor Coolant Pressure Boundary of Light Water Reactors
Part 2: Design and Analysis
KTA 3201.2

[3] K. Wallin
Fracture Toughness of Engineering Materials, Estimation and Application
EMAS Publishing, 2011

[4] ASTM E1921
Standard Test Method for Determination of Reference Temperature, T_0 for Ferritic Steels in the Transition Range

[5] A. Gundermann, H. Hein, W. Hofmann, E. Keim, H. Schnabel, T. Seibert
Determination of Fracture Mechanics Values on Irradiated Specimens of German PWR Plants – CARISMA
Final Report – Reactor Safety Research-Project No.:1501284

[6] J. Barthelmes, C. Eiselt, H. Hein, W. Hofmann, M. Kaiser, E. Keim, F. Obermeier, H. Schnabel
Extension of the Data Base of Fracture Mechanical Characteristics of Irradiated German RPV Materials – Application of the Master Curve Approach for Neutron Fluences in the Upper Bound – CARINA
Final Report – Reactor Safety Research-Project No.:1501357

[7] H. Hein, M. Kaiser, J. Kobiela, V. Lind, J. May, T. Nicak, F. Obermeier, R.Tiete
Consideration of special effects for the application of an optimized fracture mechanics approach for the RPV safety assessment – CAMERA
Final Report – Reactor Safety Research-Project No.:1501500

[8] A. Das, E. Altstadt, P. Chekhonin, M. Houska
Fracture mechanics investigation of reactor pressure vessel steels by means of sub-sized specimens - Kleinproben
Final Report – Reactor Safety Research – Project No.: 1501592B

[9] K. Wallin
The scatter in KIc-results
Engineering Fracture Mechanics 19, 6, 1085-1093

[10] X. Gao, R.H. Dodds
Constraint effects on the ductile-to-brittle transition temperature of ferritic steels: a Weibull stress model
International Journal of Fracture 102, 43-69

[11] T. Meshii, T. Yamaguchi
Applicability of the modified Ritchie-Knott-Rice failure criterion to transfer fracture toughness Jc of reactor pressure vessel steel using specimens of different thicknesses – Possibility of deterministic approach to transfer the minimum Jc for specified specimen thicknesses
Theoretical and Applied Fracture Mechanics 85, 328-344

[12] M. Yamamoto, A. Kimura, K. Onizawa, et al.
A Round Robin Program of Master Curve Evaluation Using Miniature C(T) Specimens: 3rd Report – Comparison of T_0 Under Various Selections of Temperature Conditions.
Proceedings of the ASME 2014 Pressure Vessels and Piping Conference, PVP2014-28898

[13] M. Yamamoto, N. Miura
Applicability of Miniature C(T) Specimens for the Master Curve Evaluation of RPV Weld Metal
Proceedings of the ASME 2014 Pressure Vessels and Piping Conference,PVP2015-45545

[14] K. Wallin, M. Yamamoto, U. Ehrnstén
Location of initiation sites in fracture toughness testing specimens: The effect of size and side grooves
Proceedings of the ASME 2017 Pressure Vessels and Piping Conference, PVP2016-63078

[15] T. Sugihara, K. Yoshimoto, T. Hirota, K. Tsutsumi, H. Sokamoto, T. Murakami
Applicability of miniature C(T) specimen to fracture toughness evaluation for the irradiated Japanese reactor pressure vessel steel.
Proceedings of the ASME 2017 Pressure Vessels and Piping Conference, PVP2017-66206

[16] M. Yamamoto
The Master Curve Fracture Toughness Evaluation of Irradiated Plate Material JRQ using Miniature C(T) Specimens
Proceedings of the ASME 2017 Pressure Vessels and Piping Conference, PVP2017-66085

[17] M. Sokolov
Use of Mini-CT Specimens for Fracture Toughness Characterization of Low Upper-Shelf Linde 80 Weld
Proceedings of the ASME 2017 Pressure Vessels and Piping Conference, PVP2017-65904

[18] M. Sokolov
Use of Mini-CT Specimens for Fracture Toughness Characterization of Low Upper-Shelf Linde 80 Weld before and after Irradiation
Proceedings of the ASME 2017 Pressure Vessels and Piping Conference, PVP2017-84804

[19] M. Yamamoto
Trial Study of the Master Curve Fracture Toughness Evaluation of Irradiated Plate Material JRQ using Miniature-C(T) Specimens
Proceedings of the Pressure Vessels and Piping Conference, PVP 2017-66085

[20] W. Server, M. Sokolov, M. Yamamoto, E. Carter
Inter-Laboratory results and analyses of Mini-C(T) Specimen, Testing of an Irradiated Linde 80 Weld Metal
Proceedings of the Pressure Vessels and Piping Conference, PVP 2018-84950

[21] ASTM E1820
Standard Test Method for Measurement of Fracture Toughness

[22] DIN EN ISO 7500-1: 2016-06
Metallische Werkstoffe – Kalibrierung und Überprüfung von statischen einachsigen Prüfmaschinen – Teil 1: Zug- und Druckprüfmaschinen – Kalibrierung und Überprüfung der Kraftmesseinrichtung

[23] DIN EN ISO 9513: 2013-05
Metallische Werkstoffe – Kalibrierung von Ländenänderungs-Messeinrichtungen für die Prüfung mit einachsiger Beanspruchung

[24] F.J. Zerilli, R.W. Armstrong
Dislocation-Mechanics-Based Constitutive Relations for Material Dynamics Calculations
J. Appl. Phys. Vol. 65, No. 5, March 1987, pp. 1816-1825

[25] M. Valo, T. Planman, K. Wallin
Rotation Point and K_{Jc} Estimations for Miniature CT-Specimens Based on Off-Load Line Displacement
Small Specimen Test Techniqes; 6th Volume, STP 1576 pp. 110-120

[26] DIN EN ISO 17025: 2018
Allgemeine Anforderungen an die Kompetenz von Prüf- und Kalibrierlaboratorien

[27] FAW-M 0012 Rev D.
Interne Fachanweisung, Mikroanalyse im Raster- und Durchstrahlelektronenmikroskop

[28] F.M. Beremin
A local criterion for cleavage fracture of a nuclear pressure vessel steel
Metallurgical Transaction A, 14A, Seite 2277-2287, 1983

[29] Bordet, Karstensen, Knowles, Wiesner
A new statistical local criterion for cleavage fracture in steel Part I: model presentation
Engineering Fracture Mechanics 72 (2005) 435–452

[30] PERFORM60: Prediction of the effects of radiation for reactor pressure vessel and in-core components using multi-scale modelling - 60 years' foreseen plant lifetime
Grant Agreement N° 232612, Project Final report, 2013

[31] ABAQUS, Analysis User's Manual, 2019

8. List of concerned internal reports

Report No. 1	KWU / R 413/83/146 Bestimmung der normierten reziproken Federkonstanten für CT-, DPB- und WOL-X-Proben
Report No. 2	D02-ARV-01-176-671 Bruchmechanische Untersuchungen von Reaktordruckbehälterstählen mittels Kleinprobentechnik an den Werkstoffen P7 GW, Fluenz $3.86 \cdot 10^{19} cm^{-2}$ und P370 SG, Fluenz $2.30 \cdot 10^{19} cm^{-2}$
Report No. 3	D02-ARV-01-188-080 Bruchmechanische Untersuchungen von Reaktorduckbehälterstählen mittels Kleinprobentechnik
Report No. 4	D02-ARV-01-209-059 FuE Joint Projekt Kleinproben, Fracture surface analysis

9. List of attachments

10. Attachments

Attachment 1: Design drawing 0.16T C(T) specimen

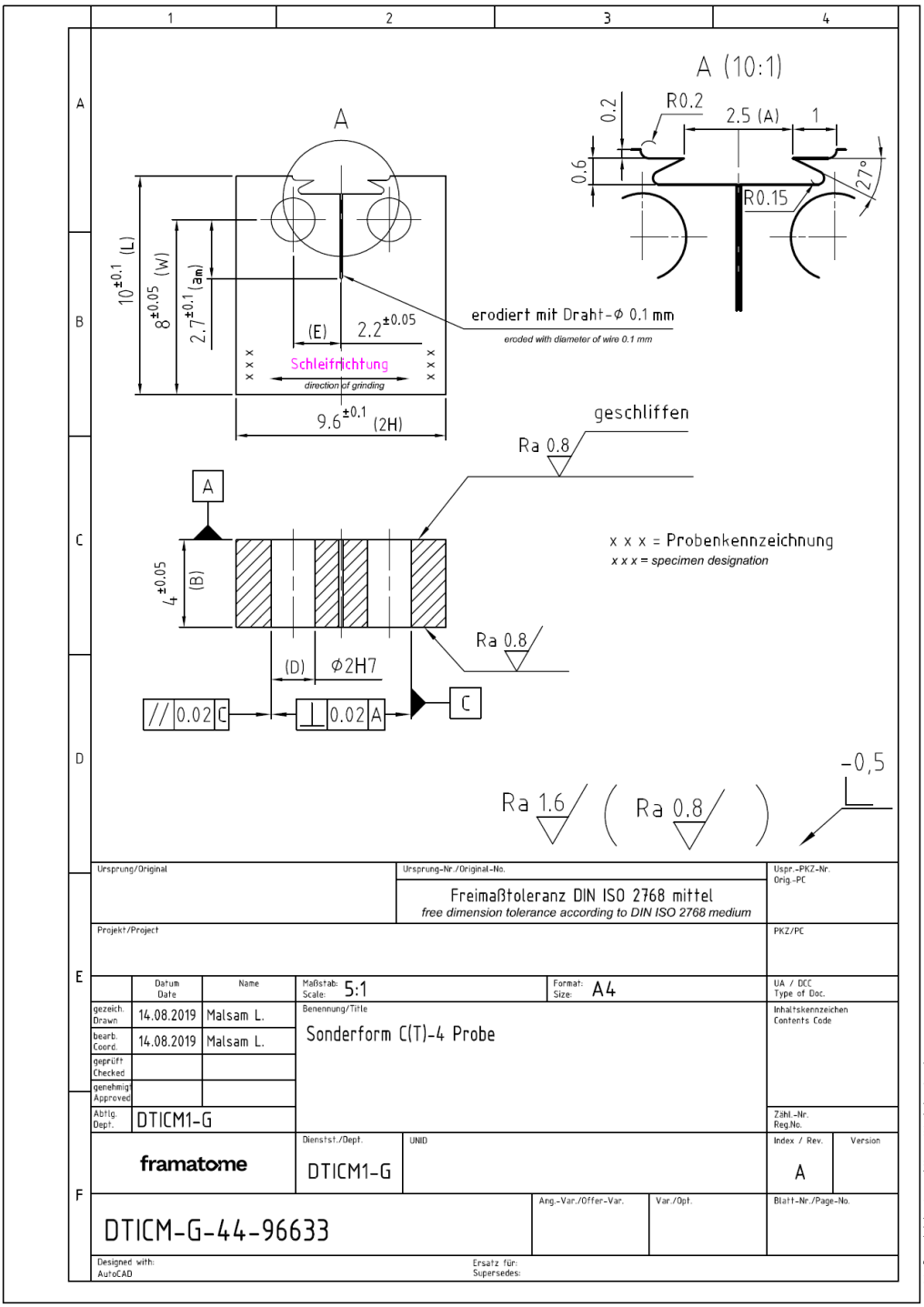

Attachment 2: Master Curve P7 BM, unirradiated
ASTM E1921-19b – CMOD to LLD conversion according KWU procedure

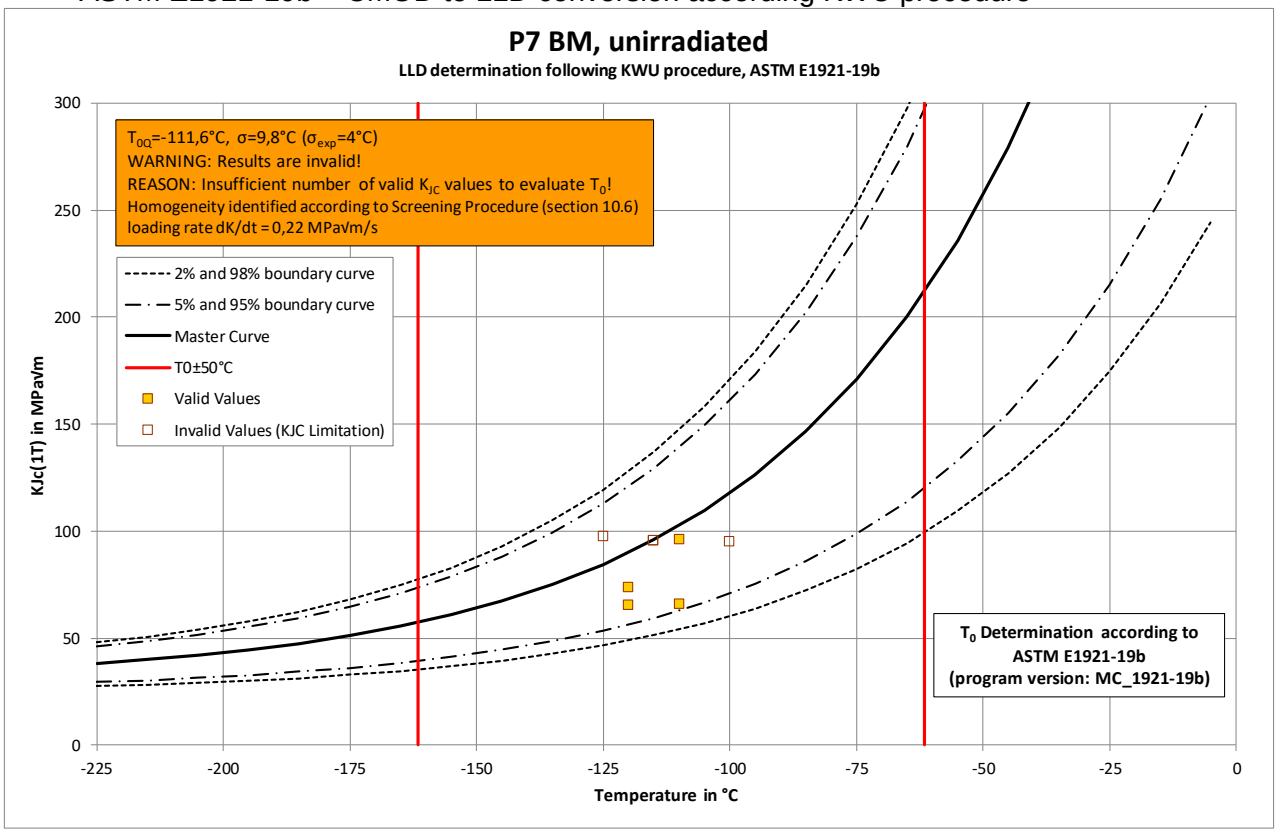

Attachment 3: Master Curve P7 BM, neutron fluence $3.86 \cdot 10^{19}$ cm^{-2} (E > 1 MeV)
ASTM E1921-19b – CMOD to LLD conversion according Hot Cells procedure

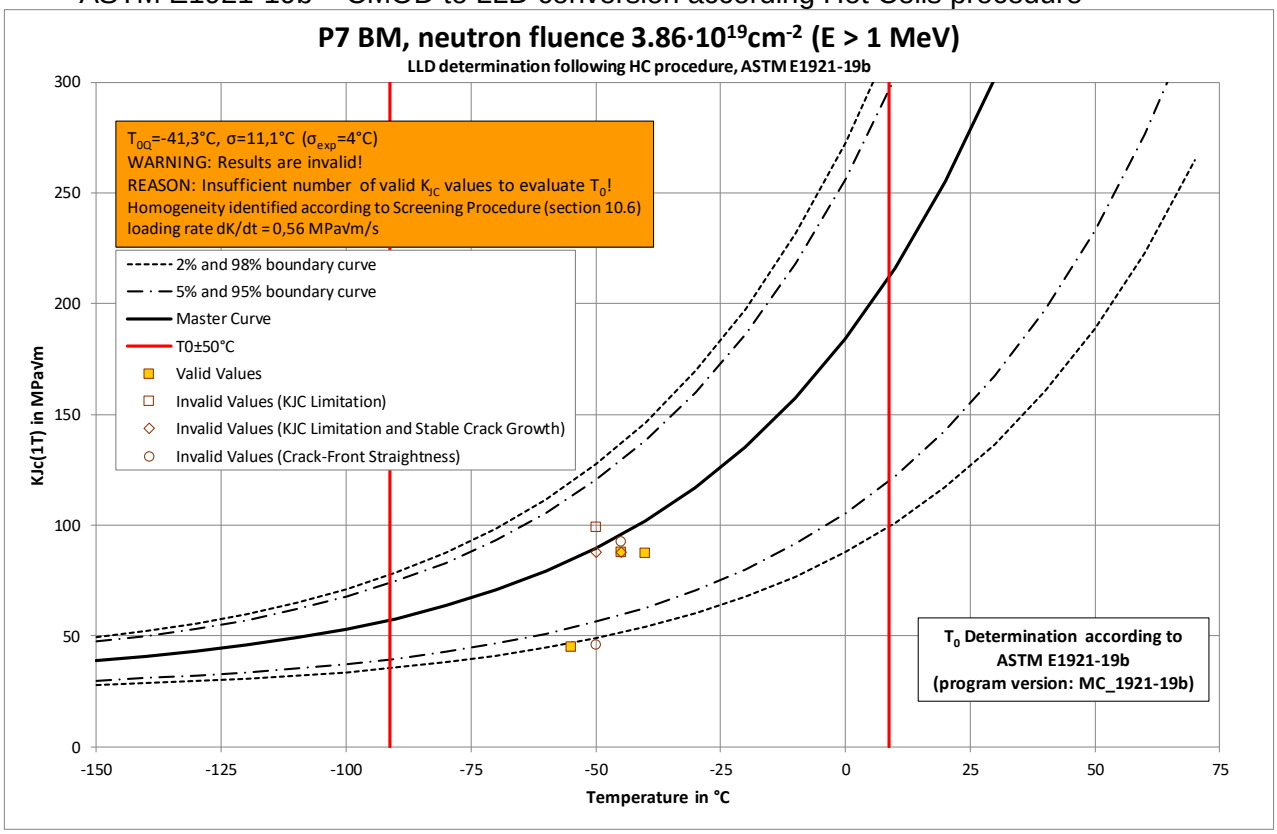

Attachment 4: Master Curve P370 WM, unirradiated
ASTM E1921-19b – CMOD to LLD conversion according KWU procedure

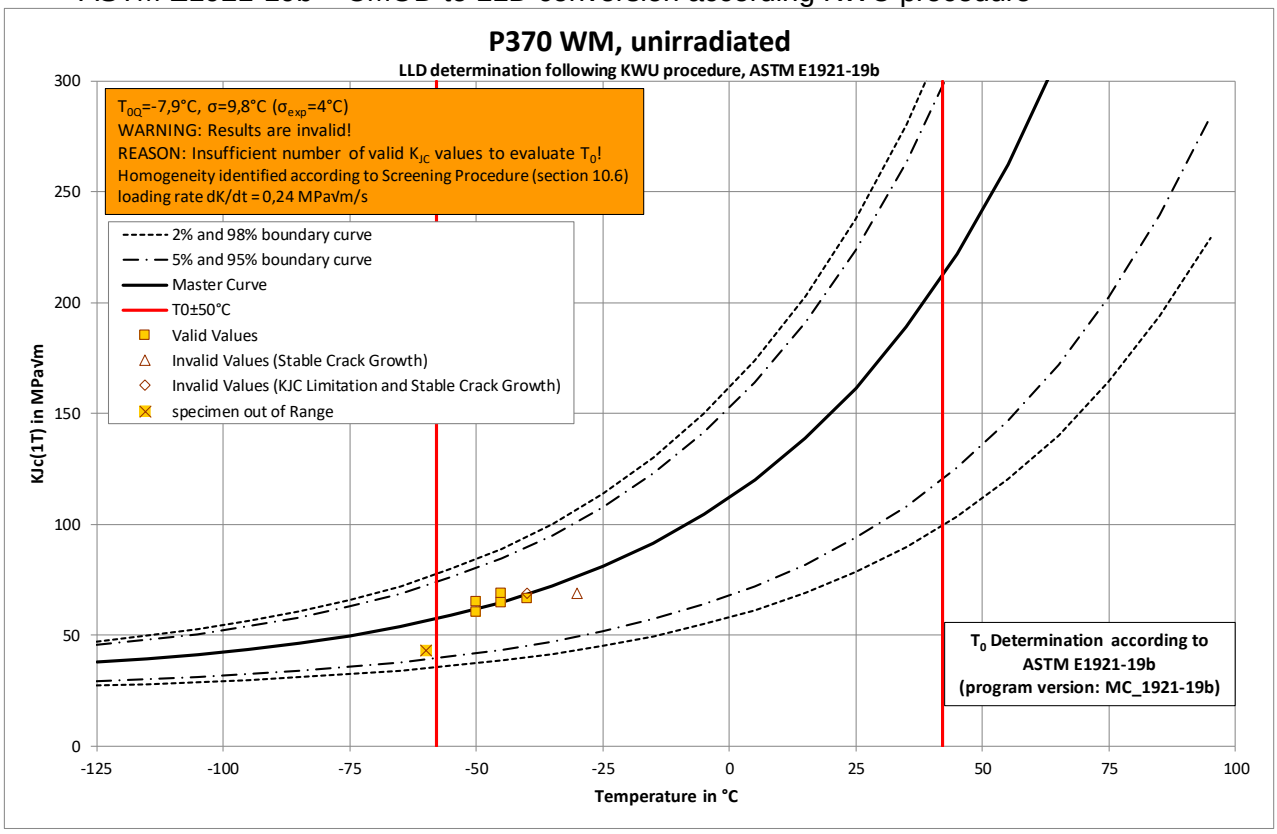

Attachment 5: Master Curve P370 WM, neutron fluence $2.30 \cdot 10^{19}$ cm^{-2} (E > 1 MeV)
ASTM E1921-19b – CMOD to LLD conversion according Hot Cells procedure

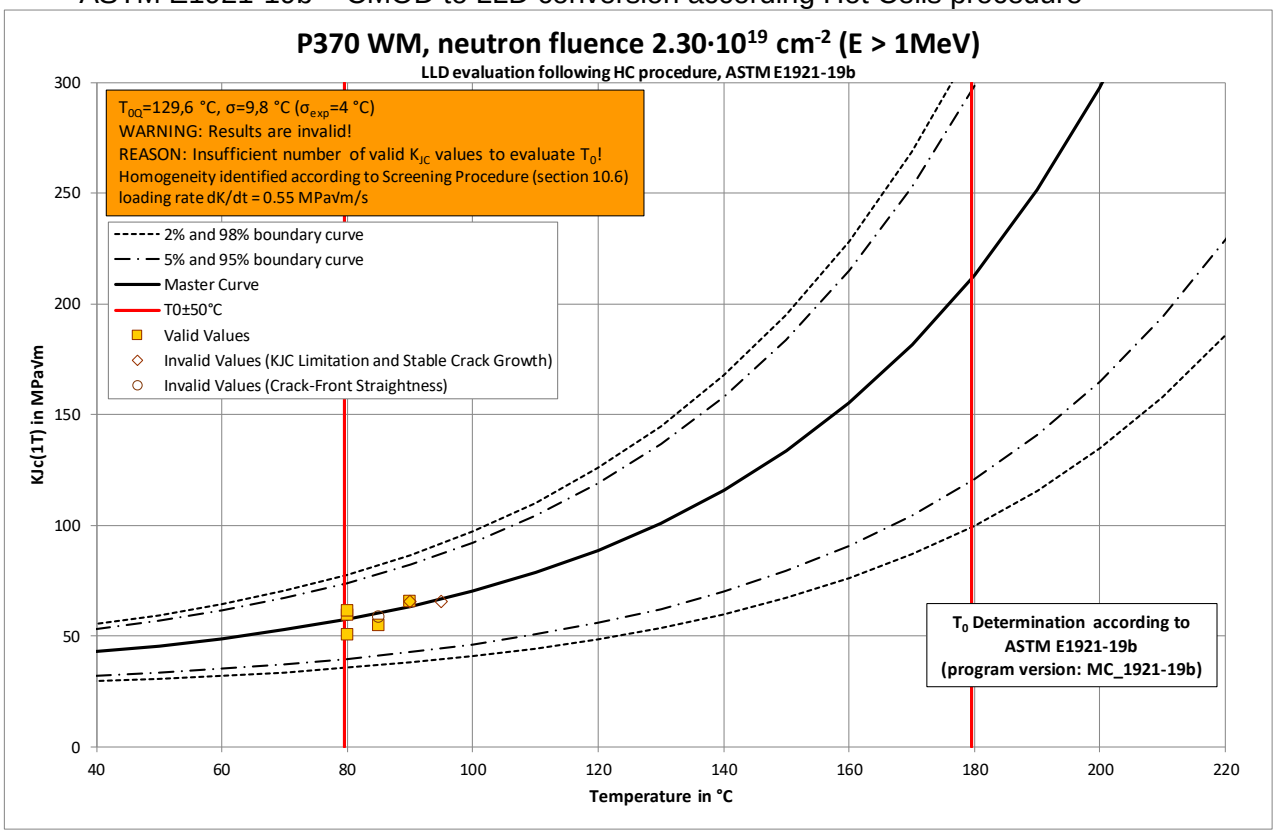

Attachment 6: Master Curve P7 BM, unirradiated
ASTM E1921-22 – CMOD to LLD conversion according ASTM E1921 procedure

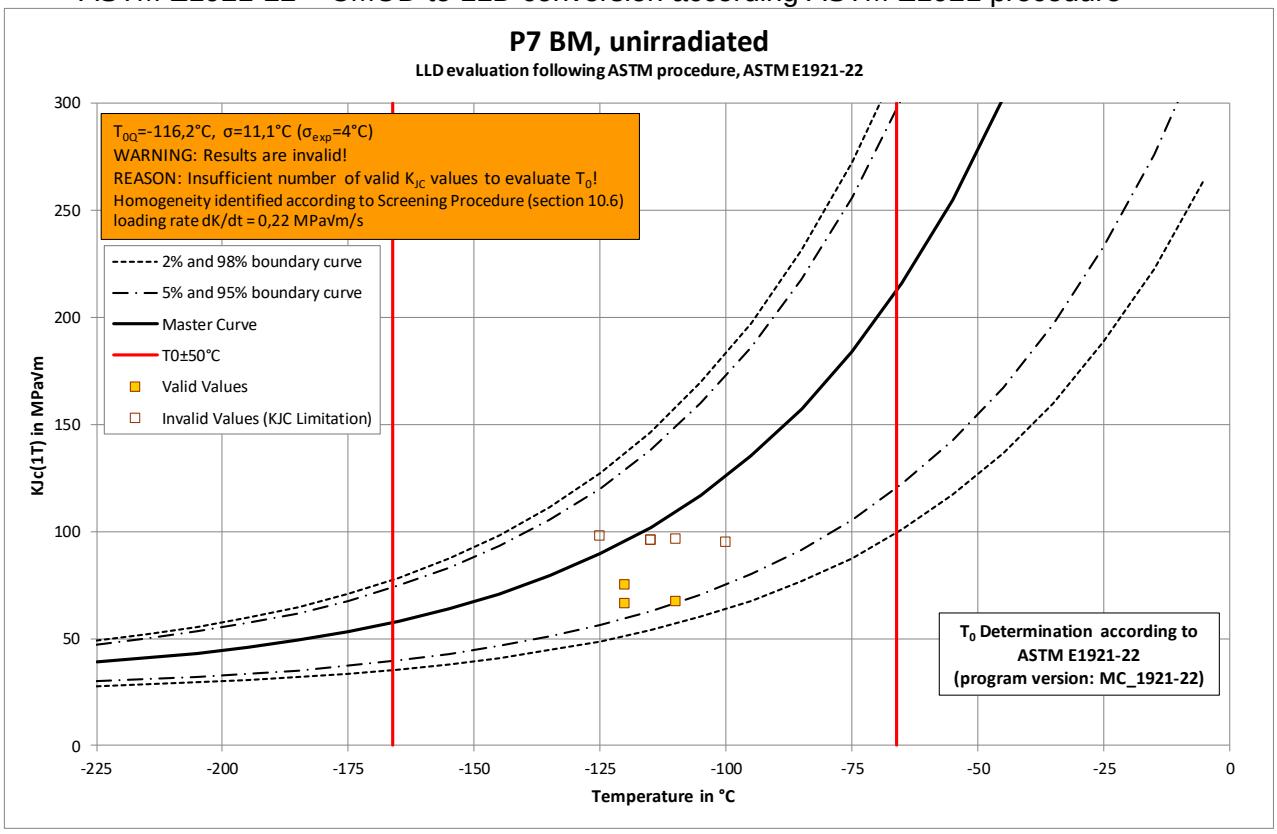

Attachment 7 :Master Curve P7 BM, neutron fluence $3.86 \cdot 10^{19}$ cm^{-2} (E > 1 MeV)
ASTM E1921-22 – CMOD to LLD conversion according ASTM E1921 procedure

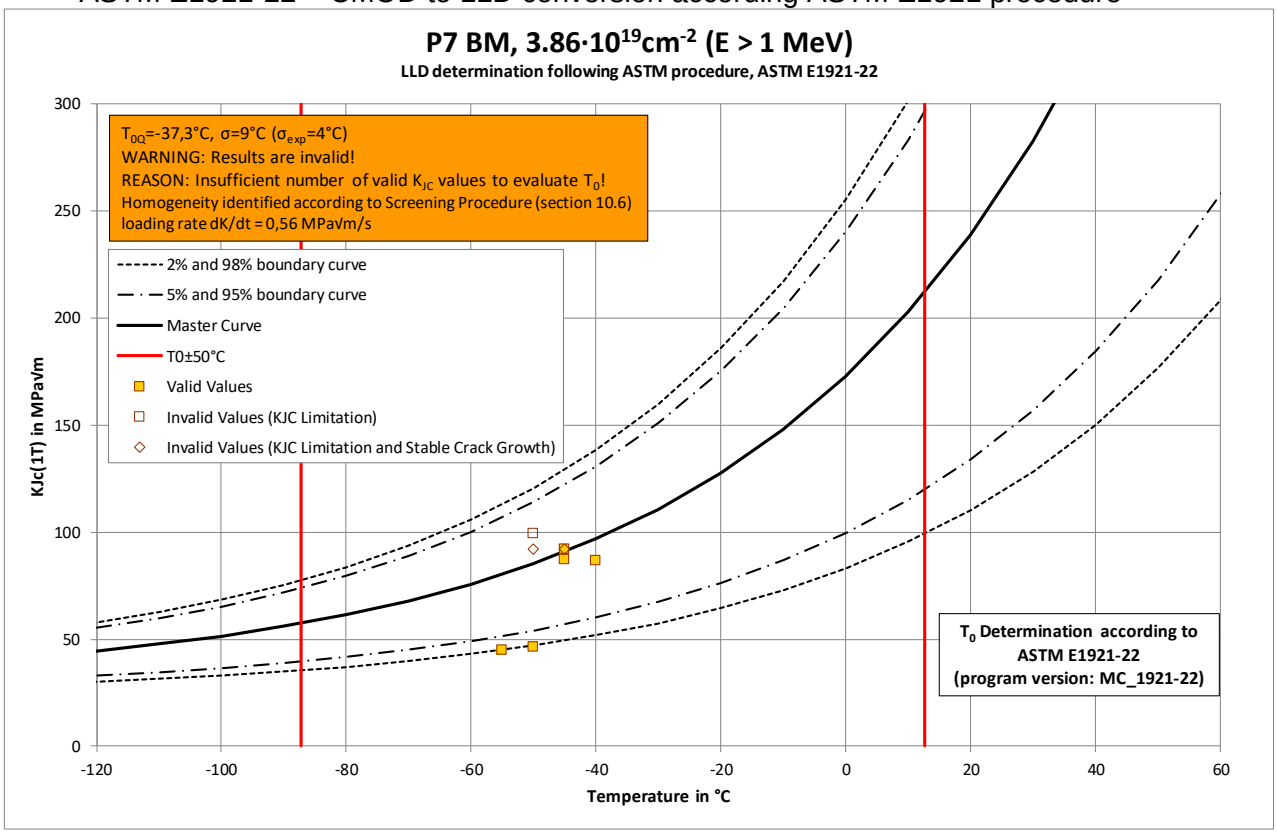

Attachment 8: Master Curve P370 WM, unirradiated
ASTM E1921-22 – CMOD to LLD conversion according ASTM E1921 procedure

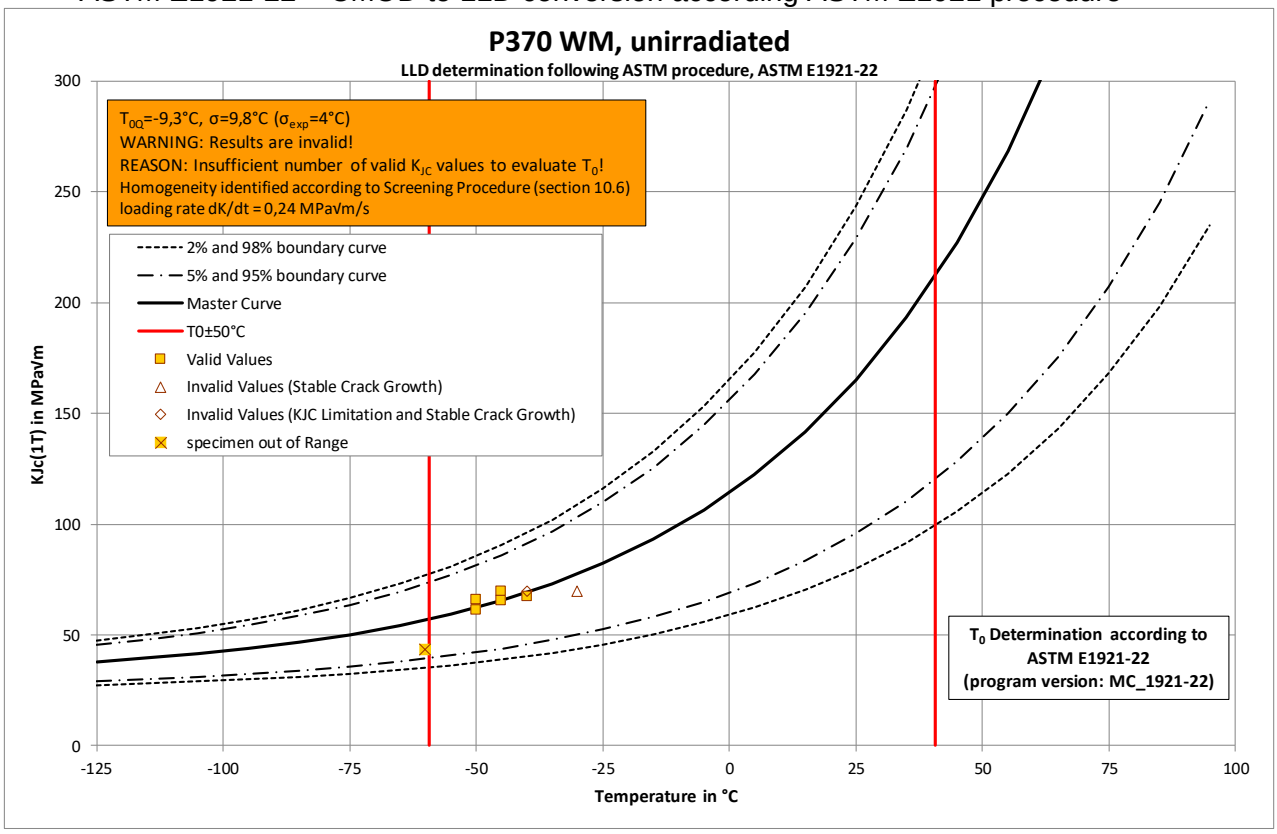

Attachment 9: Master Curve P370 WM, neutron fluence $2.30 \cdot 10^{19}$ cm^{-2} (E > 1 MeV)
ASTM E1921-22 – CMOD to LLD conversion according ASTM E1921 procedure

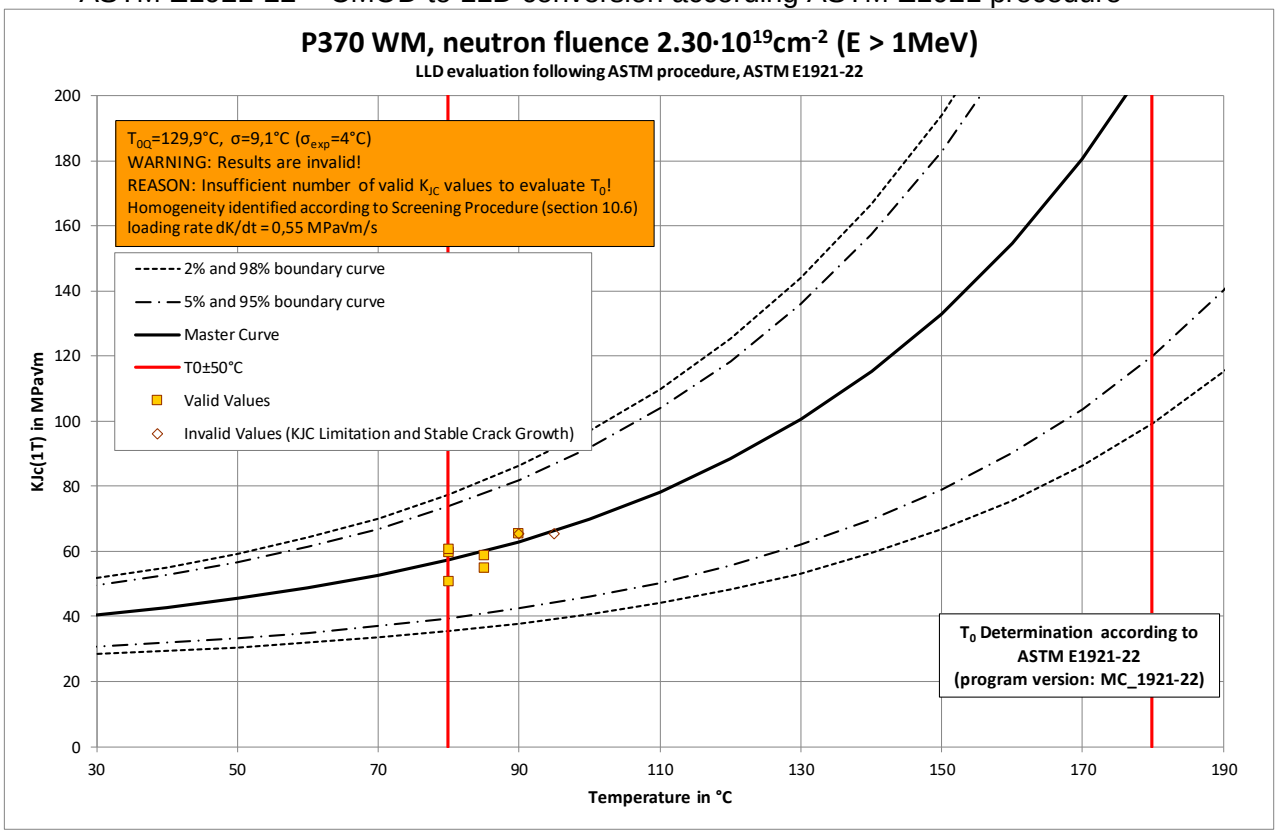

Attachment 10: Summary of fracture toughness testing results – Input for reference temperature T_0 evaluation

Material	Orientation	Specimen Designation	Used ASTM Version	Test Temperature T in [°C]	Yield stress at RT in[°C]	Yield Stress at T in [°C]	Tensile Strength at T in [°C]	Youngs Modulus in MPa	B	B_N	W	L	h	a_0	A_{pi} in [N*mm]	a_{pmax} in [mm]	Δa_p in [mm]	$\Delta a_{p,limit}$ in [mm]	K_e in [N/mm$^{3/2}$]	J_p in [N/mm]	J_e in [N/mm]	J_c in [N/mm]	K_{Jc} in [N/mm$^{3/2}$]	K_{Jc} in [MPa*√m]	$K_{Jc(limit)}$ in [MPa*√m]	$K_{Jc(1T)}$ in [MPa*√m]
ANP-5 / P370 WM	T-L	8M.3A	ASTM E 1921-22	-60	604	684	776	212400	4.04	4.04	8.01	10	2.7	4.01	31.3	0.027	0.02	0.20	1484	4.37	9.44	13.81	1795	56.8	146.0	43.2
		8M.3B		-50	604	642	740	211500	4.06	4.05	8.00	10	2.7	4.02	124.4	0.111	0.08	0.20	1796	17.41	13.87	31.29	2697	85.3	140.7	61.3
		8M.3C		-40	604	659	751	210600	4.03	4.04	8.01	10	2.71	4.08	175.9	0.075	0.05	0.20	1817	25.00	14.27	39.26	3014	95.3	141.3	67.5
		8M.3D		-30	604	648	740	209700	4.04	4.04	8.00	10	2.71	4.05	425.0	0.301	0.13	0.20	1814	60.23	14.27	74.51	4144	131.0	140.2	90.1
		8M.3E		-20		Not broken																				
		8M.3F		-45	604	659	751	211050	4.05	4.04	8.01	10	2.7	4.10	195.0	0.058	0.05	0.20	1812	27.85	14.16	42.01	3121	98.7	141.1	69.7
		8M.3G		-40		Not broken																				
		8M.3H		-50	604	642	740	211500	4.05	4.03	8.01	10	2.71	4.05	162.5	0.049	0.04	0.20	1819	22.99	14.24	37.23	2942	93.0	140.3	66.1
		8M.3J		-45	604	659	751	211050	4.02	4.00	8.01	10	2.71	4.04	156.9	0.072	0.05	0.20	1837	22.32	14.55	36.86	2924	92.5	142.2	65.7
		8M.3L		-40	604	659	751	210600	4.04	4.03	8.01	10	2.7	4.09	560.8	0.440	0.19	0.20	1808	80.00	14.12	94.12	4667	147.6	141.2	100.6
ANP-5 / P370 WM	T-L	D73A	ASTM E 1921-22	80	821	789	829	199000	4.05	3.20	8.03	9.97	2.72	4.30	69.0	0.080	0.06	0.19	2005	12.96	18.38	31.35	2618	82.8	146.5	59.7
		D73B		85	821	787	826	199000	4.06	3.20	8.03	9.97	2.69	3.77	54.1	0.040	0.03	0.21	1914	9.03	16.76	25.79	2375	75.1	156.4	54.8
		D73C		80	821	789	829	199000	4.05	4.05	8.03	9.97	2.72	3.85	93.5	0.060	0.04	0.21	2086	12.54	19.90	32.44	2664	84.2	155.1	60.6
		D73D		85	821	787	826	199000	4.01	4.01	8.03	9.97	2.71	3.89	84.0	0.050	0.04	0.21	2033	11.48	18.91	30.39	2578	81.5	154.1	58.8
		D73E		95	821	783	822	198000	4.06	4.06	8.03	9.97	2.71	3.93	1409.9	1.940	1.17	0.20	1377	192.13	8.72	200.85	6611	209.0	152.5	139.5
		D73F		90	821	785	824	198000	4.06	3.20	8.02	9.96	2.69	3.88	110.6	0.050	0.03	0.21	2074	18.96	19.76	38.72	2902	91.8	153.5	65.4
		D73G		90	821	785	824	198000	4.05	3.20	8.02	9.97	2.7	4.18	792.0	0.750	0.69	0.19	807	144.93	3.00	147.93	5673	179.4	147.9	120.7
		D73H		80	821	789	828	199000	4.05	3.20	8.02	9.98	2.7	3.94	34.6	0.050	0.03	0.20	1835	6.00	15.39	21.39	2163	68.4	153.3	50.6
ANP-3 / P7 BM	T-L	SEB1A	ASTM E 1921-22	-110	439	621	738	216900	4.04	4.04	8.01	9.96	2.71	4.03	187.3	0.040	0.03	0.20	1650	26.32	11.42	37.73	2999	94.8	140.1	67.3
		SEB1B		-100	439	621	738	216000	4.04	4.04	8.00	9.95	2.7	4.07	620.5	0.104	0.07	0.20	1758	88.14	13.02	101.16	4900	155.0	139.0	105.2
		SEB1C		-110	439	621	738	216900	4.04	4.04	8.00	9.97	2.71	3.98	527.2	0.120	0.07	0.20	1797	73.56	13.54	87.10	4556	144.1	140.8	98.4
		SEB1D		-120	439	634	781	217800	4.04	4.04	8.01	9.96	2.71	4.07	166.4	0.041	0.03	0.20	1737	23.62	12.61	36.23	2945	93.1	141.1	66.2
		SEB1E		-115	439	622	768	217350	4.04	4.04	8.01	9.96	2.71	4.05	710.1	0.106	0.07	0.20	1854	100.36	14.38	114.74	5235	165.5	140.0	111.9
		SEB1F		-120	439	643	781	217800	4.04	4.03	8.00	9.96	2.7	4.02	246.6	0.049	0.04	0.20	1792	34.76	13.41	48.17	3396	107.4	142.8	75.2
		SEB1G		-115	439	622	768	217350	4.04	4.05	8.01	9.96	2.71	4.05	1243.4	0.178	0.15	0.20	2025	175.21	17.16	192.37	6778	214.4	140.1	142.7
		SEB1H		-125	439	647	794	218250	4.05	4.04	8.00	9.97	2.7	4.05	560.1	0.083	0.06	0.20	1903	79.24	15.11	94.34	4757	150.4	142.9	102.4
ANP-3 / P7 BM	T-L	BA25A	ASTM E 1921-22	-50	596	656	778	207000	4.04	3.20	8.02	9.97	2.71	3.78	710.8	0.180	0.13	0.21	2093	119.13	19.26	138.39	5611	177.4	145.3	119.4
		BA25B		-50	596	656	778	207000	4.05	4.05	8.03	9.97	2.71	3.68	42.2	0.080	0.03	0.22	1590	5.47	11.11	16.58	1942	61.4	147.1	46.2
		BA25C		-45	596	651	773	207000	4.03	4.03	8.00	10.01	2.71	3.77	455.9	0.090	0.06	0.21	2017	60.88	17.89	78.77	4233	133.9	144.5	91.9
		BA25D		-45	596	651	773	207000	4.04	4.04	8.02	9.99	2.72	4.23	1327.5	0.460	0.28	0.19	2024	194.84	18.01	212.85	6958	220.0	136.8	146.3
		BA25E		-45	596	651	773	207000	4.05	3.19	8.01	10	2.72	3.91	300.7	0.080	0.06	0.21	2015	52.08	17.85	69.92	3988	126.1	142.3	87.1
		BA25F		-40	596	646	768	207000	4.04	3.20	8.03	10	2.71	4.18	295.2	0.050	0.04	0.19	1866	53.91	15.31	69.22	3968	125.5	137.3	86.6
		BA25G		-50	596	656	778	207000	4.02	3.19	8.01	9.96	2.69	3.95	921.9	0.460	0.33	0.20	1962	161.29	16.92	178.20	6367	201.3	142.1	134.4
		BA25H		-55	596	662	784	207000	4.05	3.20	8.03	9.96	2.68	4.16	29.0	0.010	0.00	0.19	1532	5.27	10.31	15.59	1883	59.5	139.4	45.0

Attachment 11: Inter-Laboratory Comparison, P7 BM unirradiated condition

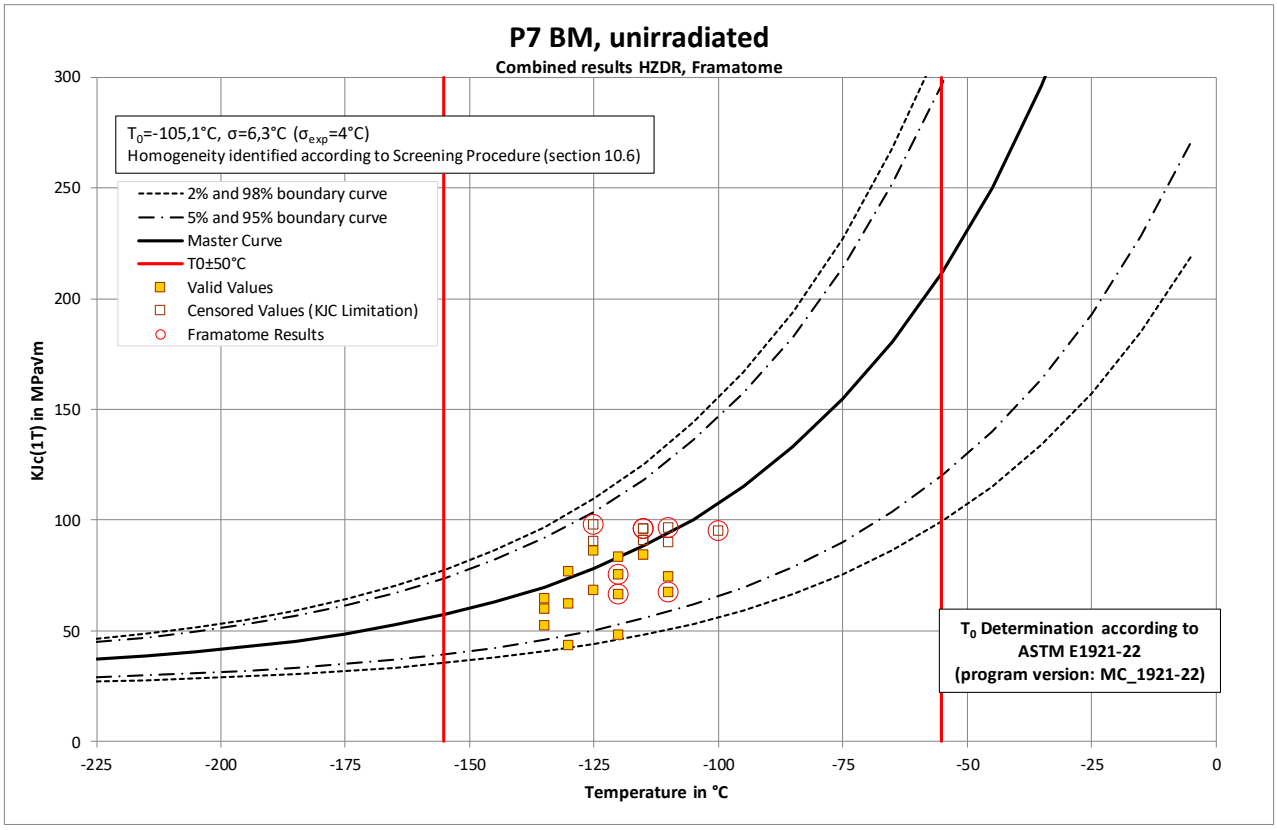

Attachment 12: Inter-Laboratory Comparison, P7 BM, neutron fluence $3.86 \cdot 10^{19}$ cm^{-2} (E > 1 MeV)

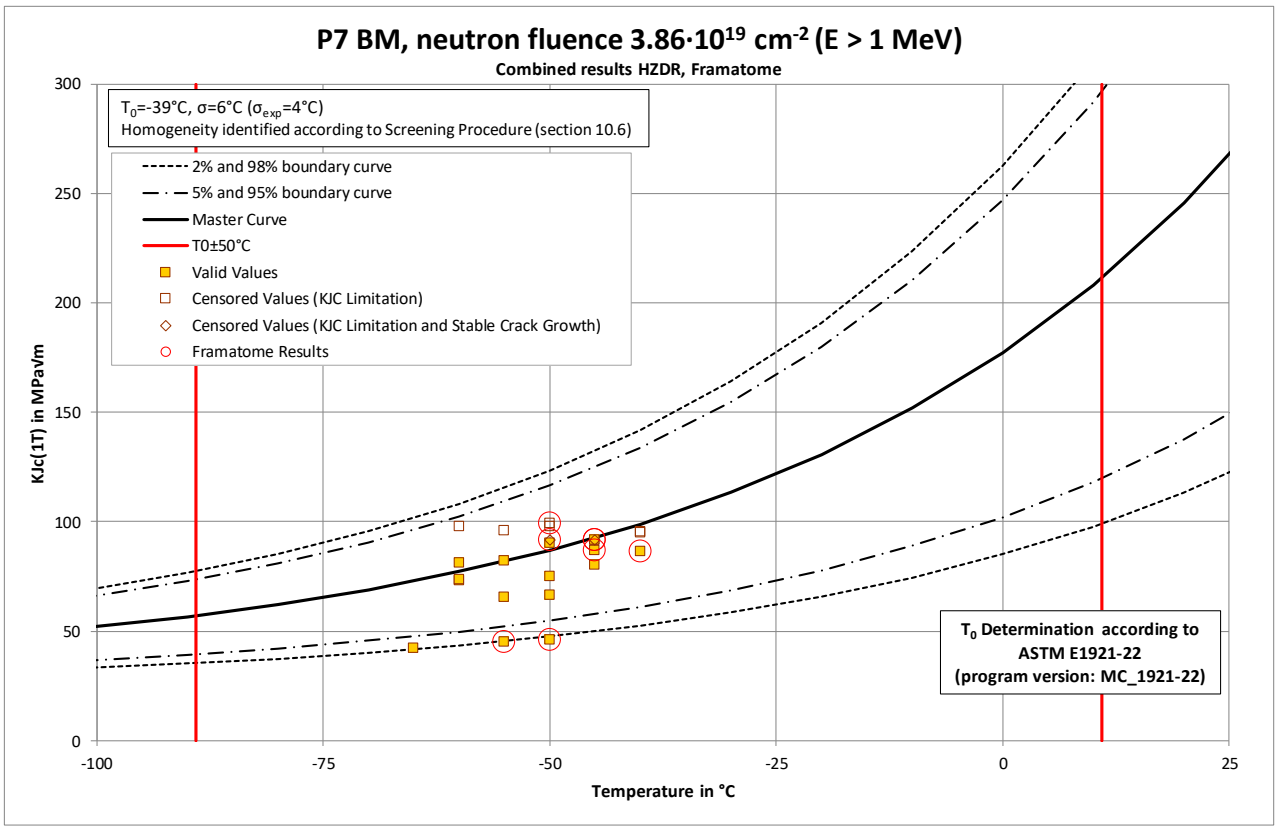

Attachment 13: Fracture surface of P370 BM samples in unirradiated conditions; the red arrows indicate the position of the crack inition site

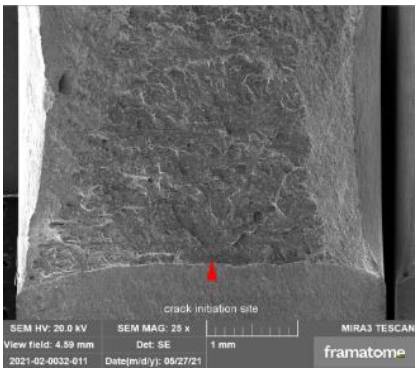

8M.3A

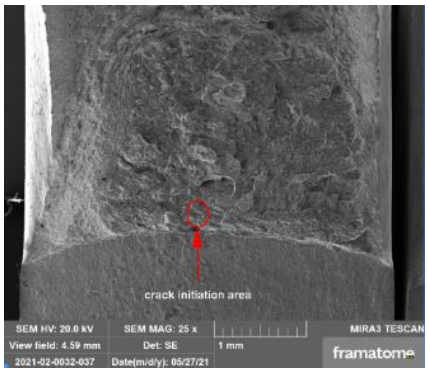

8M.3B

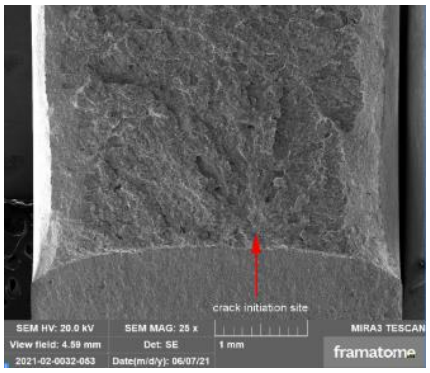

8M.3C

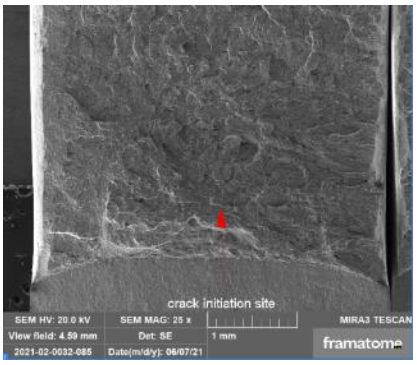

8M.3D

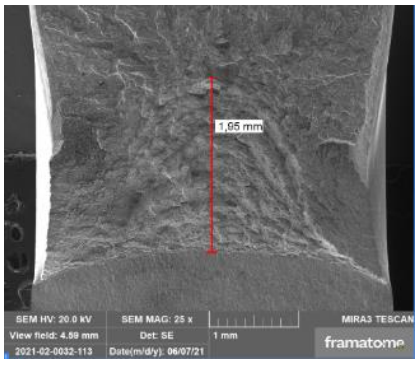

8M.3E

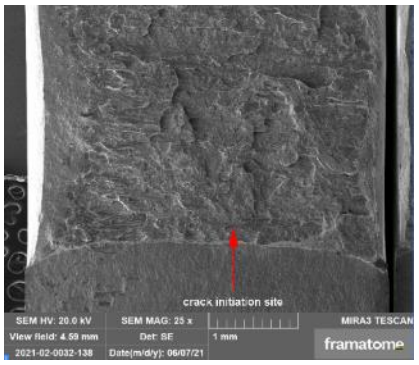

8M.3F

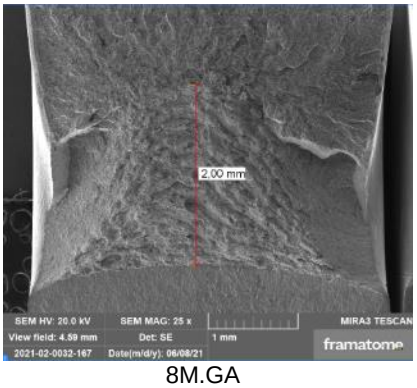

8M.GA

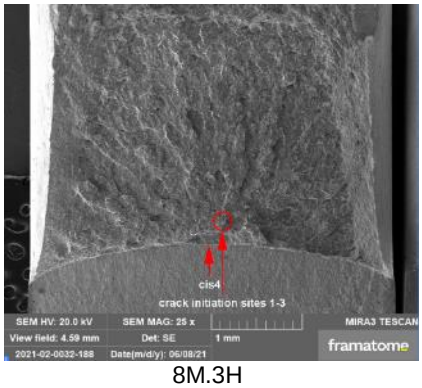

8M.3H

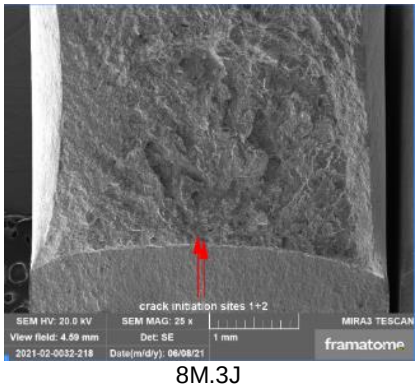

8M.3J

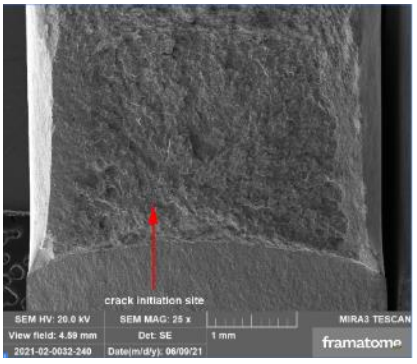

8M.3L

Attachment 14: Fracture surface characteristics of P370 WM samples in unirradiated conditions; Part 1

Specimen designation	test temp.	macroscopic fracture appearance	main fracture mode
8M.3A left side (side 1) P370 WM	-60 °C	the fracture is slightly asymmetric; on both sides slightly necking and shear lips; right side broader; shear lip at transition zone to test fracture;	mostly cleavage fracture with small intergranular areas; shear lips
8M.3B left side (side 1) P370 WM	-50 °C	the fracture is slightly asymmetric; left side slightly more necking than right side; on both sides shear lips, left side broader;	mixture: cleavage fracture (right half) and a mixture of cleavage and intergranular structures (left half); flanks with dimple structure areas and shear lips
8M.3C left side (side 1) P370 WM	-40 °C	the fracture is quite symmetric; on both sides slightly necking and shear lips;	mostly cleavage fracture with small intergranular areas; shear lips
8M.3D left side (side 1) P370 WM	-30 °C	the fracture is slightly asymmetric; on both sides insignificant necking, left side slightly more than right side; left side broader shear lip; right side partial slim and partial insignificant shear lips	mostly cleavage fracture with small intergranular areas; shear lips
8M.3E left side (side 1) P370 WM	-20 °C	the fracture is quite symmetric; on both sides necking and shear lips; approx. 2 mm stable crack growth	mostly dimple fracture
8M.3F left side (side 1) P370 WM	-45 °C	the fracture is slightly asymmetric; on both sides insignificant necking, left side slightly more than right side; left side broader shear lip; right side partial slim and partial insignificant shear lips	mostly cleavage fracture with small intergranular areas (centre and right half) and a mixture of intergranular and supposedly interdentritic fracture structures with cleavage structures (left half); flanks with dimple structure areas and shear lips
8M.3G left side (side 1) P370 WM	-40 °C	the fracture is quite symmetric; on both sides necking and shear lips; approx. 2 mm stable crack growth	mostly dimple fracture
8M.3H left side (side 1) P370 WM	-50 °C	the fracture is quite symmetric; on both sides slightly necking and shear lips	mostly cleavage fracture with small intergranular areas; shear lips
8M.3J left side (side 1) P370 WM	-45 °C	the fracture is slightly asymmetric; left side slightly more necking than right side; left side broader shear lip	mostly cleavage fracture with small intergranular areas; shear lips
8M.3L left side (side 1) P370 WM	-40 °C	the fracture is slightly asymmetric; both sides slightly necking and shear lips; left side slightly broader shear lip	mostly cleavage fracture with small intergranular areas; shear lips

Attachment 15: Fracture surface characteristics of P370 WM samples in unirradiated conditions; Part 2

Specimen designation	test temp.	presence of other fracture modes	stretch zone width (mean of 10 measurements at 5 positions)
8M.3A left side (side 1) P370 WM	-60 °C	few small areas show tensile dimples at the transition precrack/test fracture; left side areas with supposedly interdentritic structures	approx. 10 µm
8M.3B left side (side 1) P370 WM	-50 °C	small irregular seam of tensile dimples at the transition precrack/test fracture	approx. 24 µm
8M.3C left side (side 1) P370 WM	-40 °C	small irregular seam of tensile dimples at the transition precrack/test fracture; partial small dimple structure areas in the cleavage fracture;near outer wall slightly bigger intergranular structure areas	approx. 16 µm
8M.3D left side (side 1) P370 WM	-30 °C	at the transition precrack/test fracture irregular seam of tensile dimples, larger dimple structure area in the centre;partial larger dimple areas in between the cleavage test fracture; partial slightly larger intergranular areas	approx. 26 µm
8M.3E left side (side 1) P370 WM	-20 °C	partial tendency to cleavage facets or facet areas	approx. 24 µm
8M.3F left side (side 1) P370 WM	-45 °C	small irregular seam of tensile dimples at the transition precrack/test fracture	approx. 21 µm
8M.3G left side (side 1) P370 WM	-40 °C	partial tendency to cleavage facets or facet areas	approx. 21 µm
8M.3H left side (side 1) P370 WM	-50 °C	smaller irregular seam of tensile dimples at the transition precrack/test fracture; right side larger areas of intergranular structures	approx. 16 µm
8M.3J left side (side 1) P370 WM	-45 °C	small irregular seam of tensile dimples at the transition precrack/test fracture; left side bigger areas of intergranular structures	approx. 20 µm
8M.3L left side (side 1) P370 WM	-40 °C	at the transition precrack/test fracture irregular seam of tensile dimples, larger dimple area in the centre; partial slightly larger intergranular areas between the cleavage fracture in the centre area	approx. 22 µm

Attachment 16: Fracture surface of P7 WM samples in unirradiated conditions; the red arrows indicate the position of the crack inition site

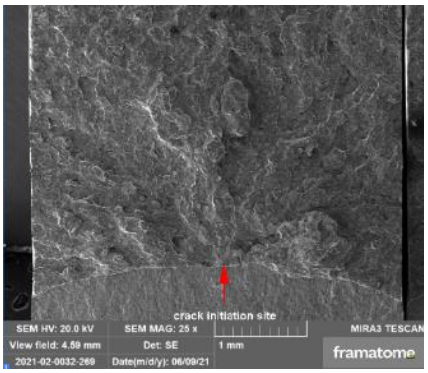

SEB1A

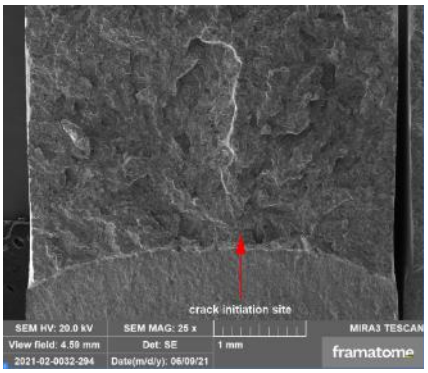

SEB1B

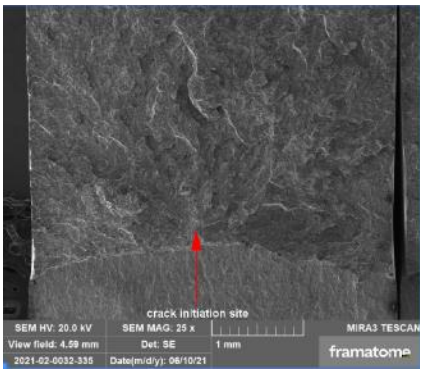

SEB1C

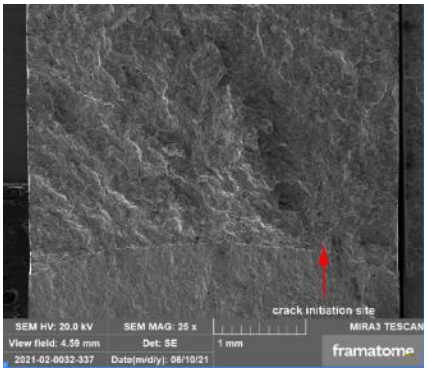

SEB1D

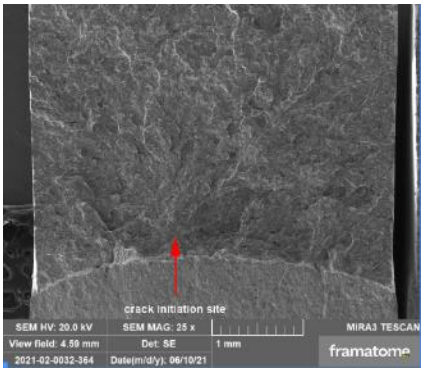

SEB1E

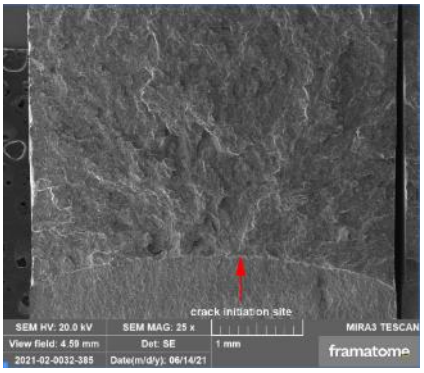

SEB1F

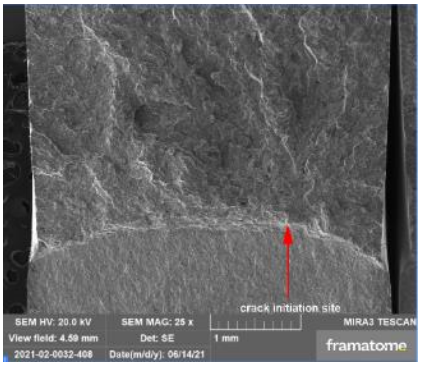

SEB1G

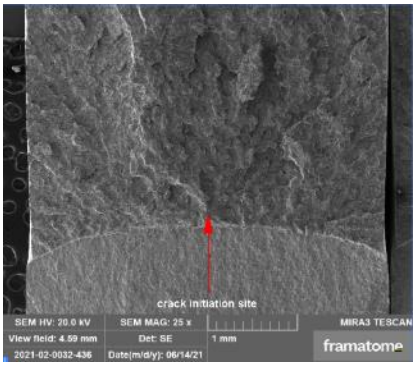

SEB1H

Attachment 17: Fracture surface characteristics of P7 WM samples in unirradiated conditions

Specimen designation	test temp.	macroscopic fracture appearance	main fracture mode	presence of other fracture modes	stretch zone width (mean of 10 measurements at 5 positions)
SEB1A left side (side 1) P7 BM	-110 °C	the fracture is quite symmetric; on both sides insignificant necking; no shear lips	mostly cleavage fracture	almost no, partial very fine seam of tensile dimple at the transition precrack/test fracture; small intergranular structure areas in the precrack	approx. 13 µm
SEB1B left side (side 1) P7 BM	-100 °C	the fracture is quite symmetric; on both sides insignificant necking; no shear lips	mostly cleavage fracture	irregular seam of tensile dimple at the transition precrack/test fracture; small intergranular structure areas in the precrack and test fracture	approx. 19 µm
SEB1C left side (side 1) P7 BM	-110 °C	the fracture is quite symmetric; on both sides insignificant necking; no shear lips	mostly cleavage fracture	almost no, partial fine seam of tensile dimple at the transition precrack/test fracture; small intergranular structure areas in the precrack and test fracture	approx. 14 µm
SEB1D left side (side 1) P7 BM	-120 °C	the fracture is slightly asymmetric; on both sides insignificant necking; no shear lips	mostly cleavage fracture	almost no, partial very fine seam of tensile dimple at the transition precrack/test fracture; small intergranular structure areas in the precrack and test fracture	approx. 13 µm
SEB1E left side (side 1) P7 BM	-115 °C	the fracture is quite symmetric; on both sides quite slightly necking near the transition precrack/test fracture; no shear lips	mostly cleavage fracture	almost no, partial irregular smaller seam of tensile dimple at the transition precrack/test fracture; small intergranular structure areas in the precrack and test fracture	approx. 24 µm
SEB1F left side (side 1) P7 BM	-120 °C	the fracture is quite symmetric; on both sides insignificant necking; no shear lips	mostly cleavage fracture	almost no, partial irregular smaller seam of tensile dimple at the transition precrack/test fracture; small intergranular structure areas in the precrack and test fracture	approx. 13 µm
SEB1G left side (side 1) P7 BM	-115 °C	the fracture is quite symmetric; on both sides quite slightly necking near the transition precrack/test fracture; no shear lips	mostly cleavage fracture	seam of tensile dimple at the transition precrack/test fracture; small intergranular structure areas in the precrack and test fracture	approx. 29 µm
SEB1H left side (side 1) P7 BM	-125 °C	the fracture is quite symmetric; on both sides quite slightly necking near the transition precrack/test fracture; no shear lips	mostly cleavage fracture	almost no, partial irregular smaller seam of tensile dimple at the transition precrack/test fracture; small intergranular structure areas in the precrack and test fracture	approx. 24 µm

Attachment 18: Fracture surface of P370 WM, neutron fluence $3.86 \cdot 10^{19}$ cm^{-2} (E > 1 MeV); the red arrows indicate the position of the crack inition site

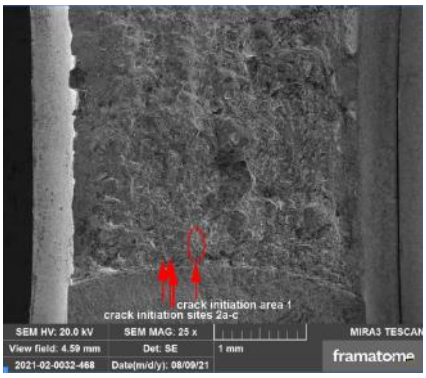

D73A

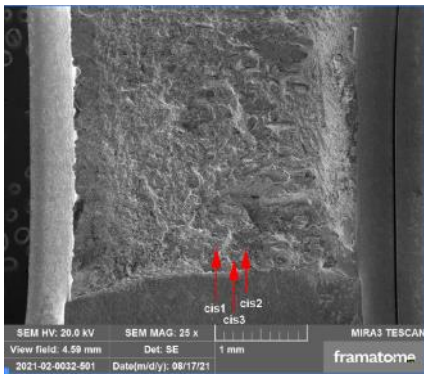

D73B

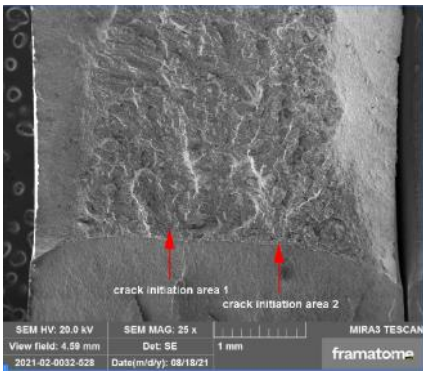

D73C

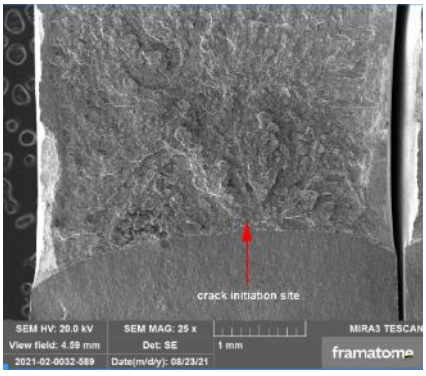

D73D

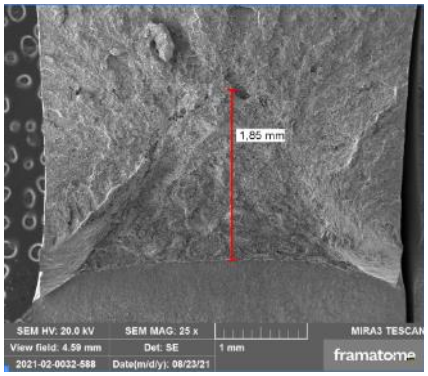

D73E

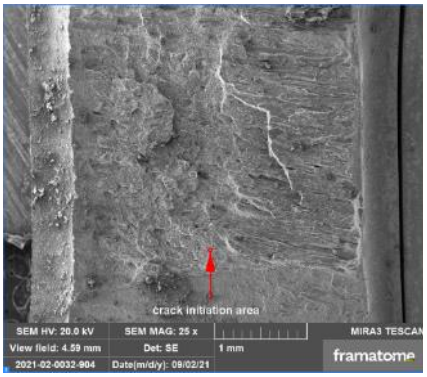

D73F

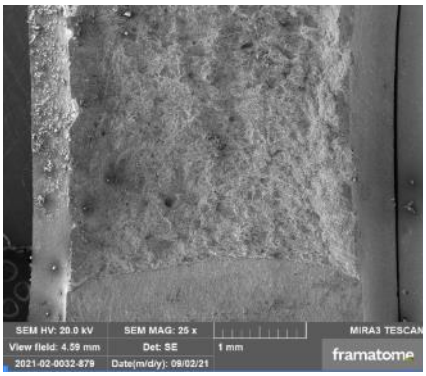

D73G

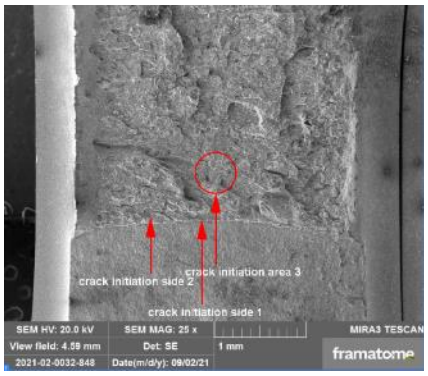

D73H

Attachment 19: Fracture surface characteristics,
P370 WM samples neutron fluence $3.86 \cdot 10^{19}$ cm^{-2} (E > 1 MeV); Part 1

Specimen designation	test temp.	macroscopic fracture appearance	main fracture mode
D73A left side (side 1) P370 WM	80 °C	the fracture is slightly asymmetric; on both sides slightly necking and shear lips;	left side mostly cleavage fracture with small intergranular areas; centre to right side mixed fracture with mostly intergranular structures and with cleavage and dimple structure areas; shear lips
D73B left side (side 1) P370 WM	85 °C	the fracture is slightly asymmetric; on both sides slightly necking and shear lips	mostly cleavage fracture mixed with larger dimple and smaller intergranular structure areas; flanks with dimple structure areas and shear lips
D73C left side (side 1) P370 WM	80 °C	the fracture is quite symmetric; on both sides slightly necking and shear lips;	left side to centre mostly cleavage fracture with intergranular and dimple areas; between centre and right side mostly intergranular structure areas mixed with cleavage and dimple areas; shear lips
D73D left side (side 1) P370 WM	85 °C	the fracture is slightly asymmetric; on both sides insignificant necking; on both sides slim irregular shear lips	mostly cleavage fracture
D73E left side (side 1) P370 WM	95 °C	the fracture is quite symmetric; on both sides slightly necking and shear lips; approx. 1,85 mm stable crack growth	mostly dimple fracture
D73F [1] left side (side 1) P370 WM	90 °C	the fracture is quite asymmetric; on both sides insignificant necking; left side slim shear lip; right side partial slim and partial insignificant shear lips	left half predominant cleavage fracture with smaller intergranular and numerous dimple structure areas; right half predominant supposedly interdentritic fracture structures with cleavage and dimple structure areas
D73G [1] left side (side 1) P370 WM	90 °C	the fracture is slightly asymmetric; on both sides slightly necking and shear lips; complete fracture stable crack growth with dimple structure	mostly dimple fracture
D73H [1] left side (side 1) P370 WM	80 °C	the fracture is slightly asymmetric; on both sides slightly necking; on both sides shear lips, left side broader;	left side and centre mostly cleavage fracture with indicated dentritic orientation; right side broader area with intergranular structure; partial larger areas with dimple structure in between

Attachment 20: Fracture surface characteristics,
P370 WM neutron fluence $3.86 \cdot 10^{19}$ cm^{-2} (E > 1 MeV); Part 2

Specimen designation	test temp.	presence of other fracture modes	stretch zone width (mean of 10 measurements at 5 positions)
D73A left side (side 1) P370 WM	80 °C	small irregular seam of tensile dimples at the transition precrack/test fracture;	approx. 12 µm
D73B left side (side 1) P370 WM	85 °C	intense irregular seam of tensile dimples at the transition precrack/test fracture	approx. 13 µm
D73C left side (side 1) P370 WM	80 °C	intense irregular seam of tensile dimples at the transition precrack/test fracture	approx. 15 µm
D73D left side (side 1) P370 WM	85 °C	irregular seam of tensile dimples at the transition precrack/test fracture; larger intergranular areas on the left side and small intergranular and increased dimple structure areas on the right side; shear lips	approx. 12 µm
D73E left side (side 1) P370 WM	95 °C	partial larger cleavage facets or facet areas; few small intergranular structure areas, between left side and centre; irregular shear lips	approx. 14 µm
D73F [1)] left side (side 1) P370 WM	90 °C	small irregular seam of tensile dimples at the transition precrack/test fracture	approx. 14 µm
D73G [1)] left side (side 1) P370 WM	90 °C	partial numerous cleavage facets or facet areas; insular cleavage and supposedly intergranular structure area	approx. 15 µm
D73H [1)] left side (side 1) P370 WM	80 °C	smaller, partial broader irregular seam of tensile dimples at the transition precrack/test fracture; shear lips	approx. 12 µm

Attachment 21:Fracture surface of samples P7 BM, neutron fluence 3.86·1019 cm-2 (E > 1 MeV); The red arrows indicate the position of the crack initiation sites

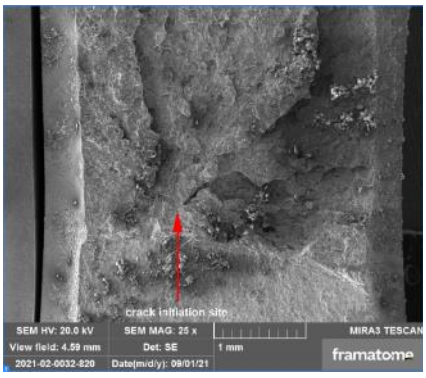

BA25A

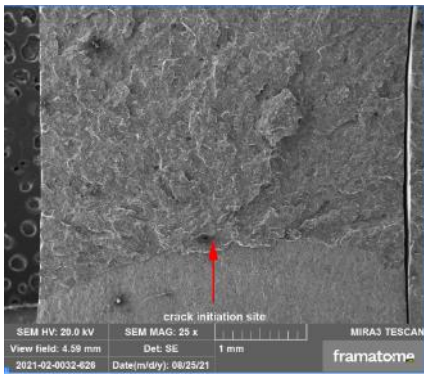

BA25B

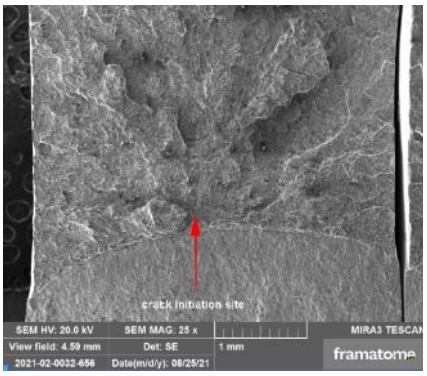

BA25C

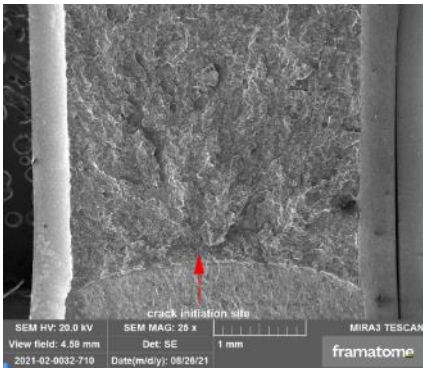

BA25D

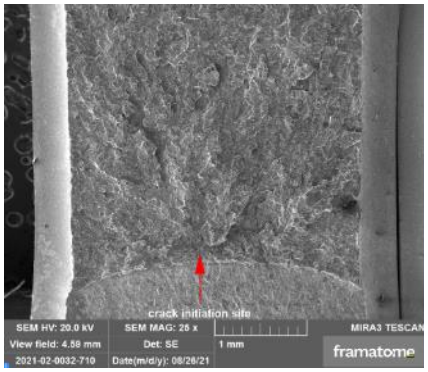

BA25E

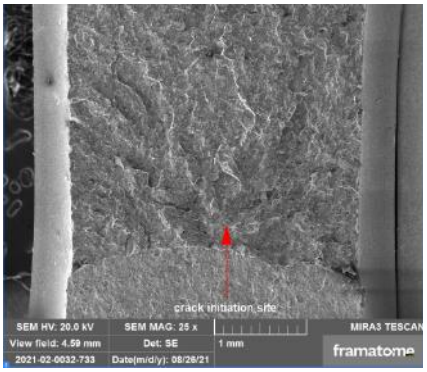

BA25F

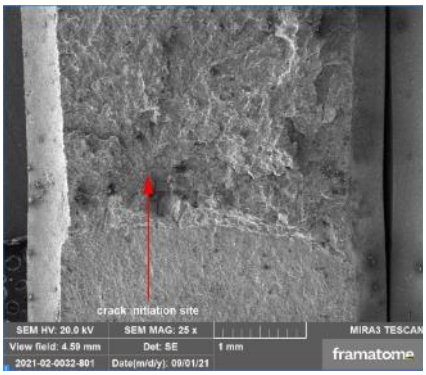

BA25G

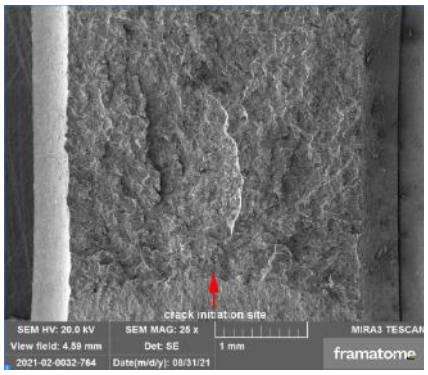

BA25H

Attachment 22: Fracture surface characteristics;
P7 BM, neutron fluence $3.86 \cdot 10^{19}$ cm^{-2} (E > 1 MeV)

Specimen designation	test temp.	macroscopic fracture appearance	main fracture mode	presence of other fracture modes	stretch zone width (mean of 10 measurements at 5 positions)
BA25A [1)] right side (side 2) szw: left side (side 1) P7 BM	-50 °C	the fracture is slightly asymmetric; on both sides no necking; no shear lips on both sides slightly necking near the transition precrack/test fracture, slightly stronger on right side (side 2); no shear lips	mostly cleavage fracture	irregular seam of tensile dimple at the transition precrack/test fracture, broarder adjacent to inculusion cluster; small intergranular structure areas in the precrack and test fracture	approx. 34 µm (measured at side 1)
BA25B left side (side 1) P7 BM	-50 °C	the fracture is slightly asymmetric, caused of asymmetrical precrack; on both sides no necking; no shear lips	mostly cleavage fracture	almost no, partial very fine seam of tensile dimple at the transition precrack/test fracture; small intergranular structure areas in the precrack and test fracture	approx. 5 µm
BA25C left side (side 1) P7 BM	-45 °C	the fracture is slightly asymmetric, caused of asymmetrical precrack; on both sides insignificant necking; no shear lips	mostly cleavage fracture	small irregular seam of tensile dimple at the transition precrack/test fracture, slightly broader in the centre; small intergranular structure areas in the precrack and test fracture	approx. 25 µm
BA25D left side (side 1) P7 BM	-45 °C	the fracture is quite symmetric; on both sides slightly necking near the transition precrack/test fracture; no shear lips	mostly cleavage fracture	small irregular seam of tensile dimple at the transition precrack/test fracture, broader in the centre with inclusion cluster; small intergranular structure areas in the precrack and test fracture	approx. 25 µm
BA25E left side (side 1) P7 BM	-45 °C	the fracture is quite symmetric; on both sides insignificant necking near the transition precrack/test fracture; no shear lips	mostly cleavage fracture	almost no, partial irregular small seam of tensile dimple at the transition precrack/test fracture; small intergranular structure areas in the precrack and test fracture	approx. 29 µm
BA25F left side (side 1) P7 BM	-40 °C	the fracture is quite symmetric; on both sides insignificant necking; no shear lips	mostly cleavage fracture	almost no, partial irregular small seam of tensile dimple at the transition precrack/test fracture, slightly broader around inclusion cluster; small intergranular structure areas in the precrack and test fracture	approx. 18 µm
BA25G [1)] left side (side 1) P7 BM	-50 °C	the fracture is slightly asymmetric; on both sides slightly necking near the transition precrack/test fracture; no shear lips	mostly cleavage fracture	irregular seam of tensile dimple at the transition precrack/test fracture, broader around inclusion cluster; small intergranular structure areas in the precrack and supposedly in the test fracture	approx. 32 µm
BA25H [1)] left side (side 1) szw: left side (side 2) P7 BM	-55 °C	the fracture is slightly asymmetric, caused of asymmetrical precrack; on both sides insignificant necking; no shear lips	mostly cleavage fracture	predominantly no dimple seam, partial fine seam of tensile dimple at the transition precrack/test fracture; small intergranular structure areas in the precrack	approx. 6 µm (measured at side 2)

Attachment 23: Crack initiation site characteristics and position, P370 WM, unirridiated condition

Specimen designation	test temp.	lateral location	distance from precrack	distance to left lateral surface	description of the fracture characteristics
8M.3A left side (side 1) P370 WM	-60 °C	crack initiation located relatively centered, single main crack initiation site;	0.05 mm	2.13 mm	initiation located in cleavage area with O MnSiAl-rich (with Ti+Zr+S+Mg) inclusion in the centre area; small intergranular areas close-by crack initiation site
8M.3B left side (side 1) P370 WM	-50 °C	crack initiation trackable to a smaller area located relatively centred, single main crack initiation area;	0.2 mm	1.89 mm	initiation located in a mixed fracture with primary cleavage and intergranular structures
8M.3C left side (side 1) P370 WM	-40 °C	crack initiation located between centre and right side, single main crack initiation site;	0.15 mm	2.43 mm	initiation located in cleavage area with O MnSiAl-rich (with Ti+S) inclusion adjacent to a small intergranular area
8M.3D left side (side 1) P370 WM	-30 °C	crack initiation located relatively centered, single main crack initiation site;	0.53 mm	2.15 mm	initiation located in cleavage area with O MnSi-rich (with Al+Ti+S) inclusion; small intergranular areas close-by crack initiation site
8M.3E left side (side 1) P370 WM	-20 °C	no crack initiation site in the test fracture;	-	-	-
8M.3F left side (side 1) P370 WM	-45 °C	crack initiation located relatively centered, single main crack initiation site;	0.53 mm	2.32 mm	initiation located in cleavage area with O MnSiAl-rich (with Ti+Zr+S+Mg) inclusion adjacent to a small intergranular area; small intergranular areas close-by crack initiation site
8M.3G left side (side 1) P370 WM	-40 °C	no crack initiation site in the test fracture;	-	-	-
8M.3H left side (side 1) P370 WM	-50 °C	crack initiation located centered, diverse crack initiation sites in a smaller area and in another level;	cis. 1-3: approx. 0.3 mm cis4: 0.02 mm	cis. 1-3: 2.13 mm	initiations located in cleavage area with small intergranular areas: cis1: small intergranular area; cis2: small intergranular area / O MnSiAl-rich (with Ti+Zr+S+Mg) inclusion; cis3: O MnSiAl-rich (with Ti+Zr+S+Mg) inclusion; cis4: inclusion adjacent to a small intergranular area
8M.3J left side (side 1) P370 WM	-45 °C	crack initiation located centered, two initiation sites nearby;	approx. 0.1 mm	1.93 mm	initiations located in cleavage area with O MnSiAl-rich (with Ti+Zr+S) inclusion; small intergranular areas close-by crack initiation site
8M.3L left side (side 1) P370 WM	-40 °C	crack initiation located between left side and centre, single main crack initiation site;	0.44 mm	1.41 mm	initiation located in cleavage area with O MnSiAl-rich (with Ti) inclusion; small intergranular areas close-by crack initiation site

Attachment 24: Crack initiation site characteristics and position, P7 BM, unirradiated condition

Specimen designation	test temp.	lateral location	distance from precrack	distance to left lateral surface	description of the fracture characteristics
SEB1A left side (side 1) P7 BM	-110 °C	crack initiation located centered, single main crack initiation site;	0.05 mm	2.10 mm	initiation located in cleavage area supposedly adjacent to an inclusion (visible depression); smaller inclusion 12 µm and bigger inclusion cluster 140 µm from crack initiation site
SEB1B left side (side 1) P7 BM	-100 °C	crack initiation located relatively centered, single main crack initiation site	0.18 mm	2.34 mm	initiation located in cleavage area, not clearly visible, whether starts at inclusion (depression visible) or at grain boundary; small intergranular areas close-by crack initiation site; bigger inclusion cluster 130 µm from crack initiation site
SEB1C left side (side 1) P7 BM	-110 °C	crack initiation located centered, single main crack initiation site;	0.16 mm	1.86 mm	initiation located in cleavage area supposedly at grain boundary; small intergranular areas close-by crack initiation site; smaller inclusion 140 µm from crack initiation site
SEB1D left side (side 1) P7 BM	-120 °C	crack initiation located between center and right side, single main crack initiation site;	0.08 mm	2.23 mm	initiation located in cleavage area adjacent to a small intergranular area; small intergranular areas close-by crack initiation site; bigger inclusion cluster 6 µm from crack initiation site
SEB1E left side (side 1) P7 BM	-115 °C	crack initiation cis1 located between left side and center, single main crack initiation site, additional secondary crack initiation sites between center and right side;	0.28 mm	1.61 mm	main initiation located in cleavage area at grain boundary; small intergranular areas close-by crack initiation site; small MnS inclusion 17 µm from crack initiation site
SEB1F left side (side 1) P7 BM	-120 °C	crack initiation located relatively centered, single main crack initiation site	0.04 mm	2.32 mm	initiation located in cleavage area position with enriched Mo at grain boundary; small intergranular areas close-by crack initiation site; bigger inclusion cluster 0,25 mm from crack initiation site
SEB1G left side (side 1) P7 BM	-115 °C	crack initiation located between center and right side, single main crack initiation site;	0.10 mm	2.88 mm	initiation located in cleavage area supposedly adjacent to a small intergranular area at the transition dimple seam to cleavage fracture near stretch zone; small intergranular areas close-by crack initiation site; bigger MnS inclusion cluster 30 µm from crack initiation site
SEB1H left side (side 1) P7 BM	-125 °C	crack initiation located centered, single main crack initiation site;	0.14 mm	2.04 mm	initiation located in cleavage area position with enriched Mo at grain boundary; small intergranular areas close-by crack initiation site; supposedly inclusion depression 5µm from crack initiation site

Attachment 25: Crack initiation site characteristics and position, P370 WM, neutron fluence $3.86 \cdot 10^{19}$ cm^{-2} (E > 1 MeV)

Specimen designation	test temp.	lateral location	distance from precrack	distance to left lateral surface	description of the fracture characteristics
D73A left side (side 1) P370 WM	80 °C	crack initiation not clearly visible, located relatively centered; single main crack initiation area and additional crack initiation sites;	approx. 0.25 mm cis2: 0.08-0.16 mm	1.80 mm	main initiation area located in a mixed fracture with cleavage, intergranular and dimpe structures; cis2a located in cleavage area with O MnSiAl-rich (with Ti+Cu) inclusion between left side and centre;
D73B left side (side 1) P370 WM	85 °C	crack initiation not clearly visible, main site located relatively centered; additional crack initiation sites between centre and right side;	cis1: 0.33 mm cis2: 0.25 mm cis3: 0.15 mm	cis1: 2.02 mm cis2: 2.23 mm cis3: 2.35 mm	main initiation located in cleavage area with O MnSiAl-rich (with Zr+Ti+S+Mg) inclusion; small intergranular areas close-by crack initiation site
D73C left side (side 1) P370 WM	80 °C	two main crack initiation areas located left and right side from centre;	cis1: approx. 0.14 mm cis2: approx. 0.11 mm	cis 1 : 1.52 mm cis2: 2.71 mm	initiation area 1 is located in cleavage area with O MnSiAl-rich (with Cu+S+Ti) inclusion adjacent to an intergranular area, between left side and centre; initiation area 2 located in an area with intergranular adjacent to cleavage and dimple structures, between centre and right side
D73D left side (side 1) P370 WM	85 °C	crack initiation located between centre and right side, single main crack initiation site;	0.13 mm	2.36 mm	initiation located in cleavage area with O MnSiAl-rich (with S+Ti+Zr) inclusion adjacent to a small intergranular area; numerous intergranular areas close-by crack initiation site
D73E left side (side 1) P370 WM	95 °C	no crack initiation site in the test fracture;	-	-	-
D73F [1] left side (side 1) P370 WM	90 °C	crack initiation located centered, single main crack initiation site for the left half; for right half no crack initiation can be located	0.24 mm	1.94 mm	initiation located in an area with cleavage and intergranular structures
D73G [1] left side (side 1) P370 WM	90 °C	no crack initiation site in the test fracture;	-	-	-
D73H [1] left side (side 1) P370 WM	80 °C	no main crack initiation visible; crack initiation site 1 and area 3 located centered;	cis1: 0.03 mm cis2: 0.08 mm area3: approx. 0.55 mm	cis1: 1.81 mm cis2: 1.63 mm area3: approx. 1.97 mm	initiation 1 and 2 located in cleavage area with smaller intergranular areas nearby; initiation area 3 located in an area with interganular adjacent to cleavage structures

Attachment 26: Crack initiation site characteristics and position, P7 BM, neutron fluence $3.86 \cdot 10^{19}$ cm^{-2} (E > 1 MeV)

Specimen designation	test temp.	lateral location	distance from precrack	distance to left lateral surface	description of the fracture characteristics
BA25A [1)] right side (side 2) szw: left side (side 1) P7 BM	-50 °C	crack initiation located between left side and centre (side 2), single main crack initiation site;	0.28 mm	2.55 mm	initiation located in cleavage area supposedly on grain boundary; larger inclusion cluster 120 µm from crack initiation site
BA25B left side (side 1) P7 BM	-50 °C	crack initiation located centered. single main crack initiation site	0.15 mm	1.89 mm	initiation located in cleavage area with an inclusion in the centre area; EDS side 2: CuSMoN-enriched (with Al+Ca); smaller inclusion and small intergranular areas close-by crack initiation site
BA25C left side (side 1) P7 BM	-45 °C	crack initiation located relatively centred. single main crack initiation site;	0.16 mm	1.85 mm	initiation located in cleavage area position with enriched Mo; small intergranular areas close-by crack initiation site; inclusion cluster 0.1 mm from crack initiation site near stretch zone
BA25D left side (side 1) P7 BM	-45 °C	crack initiation located between left side and centre. single main crack initiation site;	0.47 mm	1.48 mm	initiation located in cleavage area adjacent to a small intergranular area; small intergranular areas close-by crack initiation site; small inclusion nearby (4 µm). larger inclusion cluster 0.16 mm below crack initiation site
BA25E left side (side 1) P7 BM	-45 °C	crack initiation located centered. single main crack initiation site;	0.09 mm	1.83 mm	initiation located in cleavage area at grain boundary with enriched MoAlN; small intergranular areas close-by crack initiation site
BA25F left side (side 1) P7 BM	-40 °C	crack initiation located relatively centered. single main crack initiation site	0.27 mm	2.16 mm	initiation located in cleavage area position with slightly enriched Mg+Al at grain boundary adjacent to a small intergranular area; small intergranular areas close-by crack initiation site; inclusion cluster 0.3 mm below crack initiation site
BA25A [1)] right side (side 2) szw: left side (side 1) P7 BM	-50 °C	crack initiation located between left side and centre (side 2). single main crack initiation site;	0.28 mm	2.55 mm	initiation located in cleavage area supposedly on grain boundary; larger inclusion cluster 120 µm from crack initiation site
BA25B left side (side 1) P7 BM	-55 °C	crack initiation located centered. single main crack initiation site	0.15 mm	1.89 mm	initiation located in cleavage area with an inclusion in the centre area; EDS side 2: CuSMoN-enriched (with Al+Ca); smaller inclusion and small intergranular areas close-by crack initiation site

Attachment 27: Local approach results SE(B) 10x10,
P370 WM neutron fluence 2.25 cm^{-2} (E > 1 MeV)

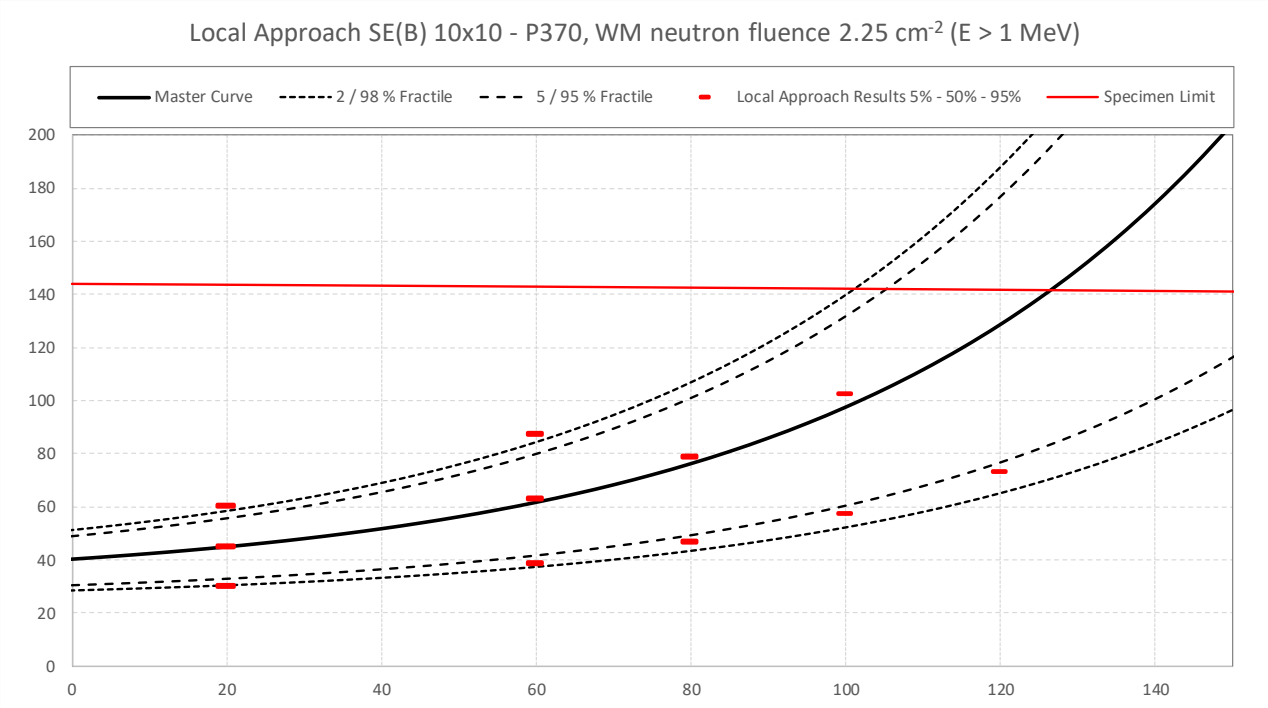

Attachment 28 Local approach results 0.16T C(T),
P370 WM neutron fluence 2.25 cm^{-2} (E > 1 MeV)